Arabian Journal of Chemistry (2020) **13**, 5691–5716

King Saud University

Arabian Journal of Chemistry

www.ksu.edu.sa
www.sciencedirect.com

ORIGINAL ARTICLE

Using Zeolite/Polyvinyl alcohol/sodium alginate nanocomposite beads for removal of some heavy metals from wastewater

Heba Isawi

Desert Research Center, Water Resources and Desert Soils Division, Hydrogeochemistry Dept., Water Desalination Unit, Egyptian Desalination Research Center of Excellence (EDRC), 1 Mathaf Al Mataria St., Cairo P.O.B. 11753, Egypt

Received 26 December 2019; accepted 10 April 2020
Available online 28 April 2020

KEYWORDS

Heavy metal removal;
Water treatment;
Zeolite nanocomposites;
Poly(vinyl alcohol)/sodium alginate beads;
Antibacterial performance

Abstract Functionalized Polyvinyl alcohol/sodium alginate (PVA/SA) beads were synthesized via blending Polyvinyl alcohol (PVA) with sodium alginate (SA) and the glutaraldehyde was used as a cross-linking agent. The zeolite nanoparticles (Zeo NPs) incorporated PVA/SA resulting Zeo/PVA/SA nanocomposite (NC) beads were synthesized for removal of some heavy metal from wastewater. The synthesizes beads were characterized via Fourier transforms infrared spectroscopy (FTIR), X-ray diffraction (XRD), particle size analyzer (PSA), and scanning electron microscope (SEM). The adsorption kinetics of the selected metal ions onto Zeo/PVA/SA NC beads followed the pseudo-first-order model (PFO) and the adsorption isotherm model was well fitted by the Langmuir model. Moreover, the thermodynamic studies were also examined; the outcomes showed that the adsorption mechanisms of the selective metal ions were endothermic, the chemical in nature, spontaneous adsorption on the surface of the Zeo/PVA/SA NC beads. The removal efficiency using Zeo/PVA/SA NC modified beads reached maximum at the pH value of 6.0 for Pb^{2+}, Cd^{2+}, Sr^{2+}, Cu^{2+}, Zn^{2+}, Ni^{2+}, Mn^{2+} and Li^{2+} with 99.5, 99.2, 98.8, 97.2, 95.6, 93.1, 92.4 and 74.5%, respectively, while the highest removal are achieved at pH = 5 for Fe^{3+} and Al^{3+} with 96.5 and 94.9%, respectively and decreased at lower or higher pH values. The survival count (%) of the E. coli cells were 34% on the SA beads, 11% on the PVA/SA, and 1% on the Zeo/PVA/SA NC modified beads, after 120 min exposure at 25 °C. Reusability experimental displays that the synthesized beads preserved a significant decrease in the sorption capacity after 10 repeating cycles. The Zeo/PVA/SA NC beads were able to eliminate 60–99.8% of Al^{3+}, Fe^{3+}, Cr^{3+}, Co^{2+}, Cd^{2+}, Zn^{2+}, Mn^{2+}, Ni^{2+}, Cu^{2+},

E-mail address: hebaessawi@hotmail.com
Peer review under responsibility of King Saud University.

Production and hosting by Elsevier

https://doi.org/10.1016/j.arabjc.2020.04.009

Li^{2+}, Sr^{2+}, Si^{2+}, V^{2+}, and Pb^{2+} ions from the natural wastewater samples collected from 10th Ramadan City, Cairo, Egypt.

1. Introduction

The Scarcity of freshwater supplies problem as a result of water contamination and dangers of climate change have greatly affected the manipulation of water resources in the worldwide [Godfray et al. 2010, Tirkey et al. 2017]. Recently, Egypt water policy aims to well manage the available water resources and preserved groundwater and surface superiority. The main sources of groundwater contamination in the 10th of Ramadan city are industrial, domestic activities, oxidation ponds, and agriculture. The waste degradation and rainfalls caused penetration of the related heavy metal ions from industrial, agricultural activities or domestic to the groundwater [Waseem et al., 2014] and have opposing effects in a short and/or long time on humans and environments. Industrial activity is one the most dangerous source of contamination of the groundwater and varies depending on the kind of industry, the method of disposing of the output, and the contents of the heavy elements [Chintalapudi et al. 2017]. Heavy metals are enzyme inhibitors, metabolic toxins and reason for the mental delay and semi-persistent brain injury. Various organic pollutants and toxic heavy metals have been discharged into the environs such as manufacturing wastes, producing dangerous water and soil pollution. Therefore, innovative treatment is significant to eliminate these contaminants, where, adsorptions are the greatest mutual technologies used in proceeding wastewater purification [Baker and Khalili 2007]. In the traditional treatment, numerous chemical techniques include water softening, filtration and extraction [Aguado et al., 2009], ion exchange, membrane separation [Wang and Chung 2006], redox, co-precipitation and chemical reduction [El-Hag Ali et al., 2008], electrodialysis, fixed and adsorption [Priya et al., 2009], adsorption via ionic liquid extraction and natural lower cost adsorbents [Abdel Salam et al., 2011]. In this research, adsorption is commonly chosen for the removal of heavy metal ions owing to its easy handling, obtainability of various adsorbents; cost efficiency, operative and high efficiency. Several adsorbents, such as minerals, activated carbon, resins, beads, aluminum hydroxide, and calcium nitrate were obtainable for heavy metal removal and reclamation. The modified adsorptive materials such as activated carbon, polymeric/composite microcapsules, polymeric sorbents, solvent saturated resins, chitosan beads, silica gel and the Zeolites nanoparticles between the most sorbent resources which have gained considerable attention for several types of metal removal [Dragan et al., 2014]. Recently, more attention has been concentrated on the utilizing of naturally obtainable low-cost materials for eliminating heavy metal ions from wastewater [Preetha and Viruthagiri 2007] due to its highly environmentally friendly and more technically achievable. In this framework, beads have developed for owing to their excellent absorption property as well as good thermal, chemical and mechanical possessions. Beads are easy networks with interstitial liquefied that capable of absorbing enormous quantities of water or biological solutions [Gonzalez et al., 2016]. In this research, various types of polymers containing synthetic and natural materials, have been informed for adsorption of heavy metal, such as agar, polyacrylamide, salt alginate, polysulfone, polyurethane, acrylamide, Poly(vinyl alcohol), amino acids, amidoxime, chitosan, silica, and polyethyleneimine have been utilized to synthesized chelating polymers, their analytical and adsorption possessions were examined [Say et al., 2002]. The greatest techniques depended on the modification of chemisorption and physisorption applications. It is identified that sodium alginates play a substantial role in metal obligatory [Park and Chae 2004]. Sodium alginate (SA) is naturally occurring polysaccharides attained from seaweeds or brown algae [Peretz et al., 2015] pertinence to the Phaeophyceae, consist of two monomeric units; a-L-guluronic acid and h-D-mannuronic acid [Agrawal et al., 2010]. SA has been attracted enormous attention presently as it has good membrane creating possessions and shows great activity with hydrogen and carbonyl (C═O) groups. The formation of alginate-goethite beads and the application in Cr(III) and Cr(VI) elimination have been stated [Chen et al., 2010]. Furthermore, it extensively displays high attraction for heavy metals, particularly for Pb (II) [Wang et al., 2016]. SA is rich in hydroxyl (OH) and carboxyl (COOH) functional groups and extra negatively charged sites, which are the foremost groups involved in heavy metal adsorption [Alfaro-Cuevas-Villanueva et al., 2014]. Additional application of SA is the fabrication of adsorbents to be used in adsorption procedures [Fang et al., 2011]. The SA was used in the creation of nanofibers for the removal of Cd^{2+} ions from aqueous solutions [Ebrahimi et al., 2019]. Rahman and Wilfred 2018 was created calcium alginate/Poly (vinyl)alcohol was used as the absorbent for Mn (VII) removal from industrial wastewater and the amount of Mn(VII) removal up to 65% from the industrial wastewater. Chuan et al., 2018 prepared adsorbent beads comprising PVA and SA via cross-linking with boric acid and calcium chloride for adsorbent of the Cr (VI) and the results revealed that adsorbent beads with 2.5 g SA and 12 g of PVA beads displayed superior Cr (VI) adsorption efficiency at 1.5 h. More often, SA is utilized for the encapsulation of various bio [Mahamadi and Zambara 2012], mineral materials such as active carbon [Choi et al., 2009], kaolin [Li et al., 2011], montmorillonite [Iliescu et al., 2014], synthetic zeolite, etc., to develop their applicability and adsorption capacities for various contaminants. Conversely, the physic-chemical possessions of SA need to be enhanced such as via polymer blends technique. Poly (vinyl alcohol) (PVA) is a nontoxic water-soluble synthetic polymer, which is extensively utilized in biochemical, medical, and industrial applications as a result of its compatibility with the alive body [Yamaura et al., 1990]. The combination of PVA in convinced hydrogel confirms its excellent water rejection possessions. PVA is a high strength polymer for the enzyme, a synthetic polymer, cell immobilization, nontoxic, and have superior mechanical possessions [De Queiroz et al.,

2006]. PVA-Alginate composites are physically powerful and stronger than the SA ones, even though both beads own water components enormously greater than their polymer components [Kobayashi, et al., 2010]. In this work, the PVA was chosen because of its good film-creating ability, biocompatibility, high hydrophilicity, nontoxicity, smooth surface, and chemical/physical stability [Isawi 2019]. The removal of heavy metals using low-cost sorbents, e.g., naturally occurring zeolites, is seen as an alternative to the revealed treatment procedures (Shalaby et al., 2018). Alike to clay minerals, isomorphic replacement of Si by Al in the three-dimensional lattice of the zeolite is the reason for a net negative charge, which is composed via replaceable cations. Zeolites are hydrated micro-porous alumino-silicate constituents with small pore size and high absorptivity commonly used as a commercial adsorbent in gas purification and ion-exchange separation [Payra and Dutta 2003] which owing cage-like configurations with inner and outer surface regions of up to numerous hundred square meters per gram (100 m^2/g) and cation exchange abilities of up to numerous milliequivalents per kilogram (meq/kg). Recently, zeolite has an extensive record as most inorganic constituents are added as fillers into the polymeric materials for declining heavy metals and biological quantity in wastewater [Rihayat, et al., 2007, Zendehde et al., 2016]. Zeolite is also utilized as a molecular sieve and as a catalyst in the manufacture of laundry cleansing agents, in agriculture determinations for the preparation of innovative ingredients and new to create the nanocomposites [Jahangirian et al., 2013]. Both natural and synthetic nano zeolites are utilized in the industry as soil modifiers, molecular sieves, ion exchangers and adsorbents [Rushdi et al., 1999]. Foremost improvements have been touched via surface modification of these nanoparticles.

To this objective, SA impeded Zeo NPs were added in a PVA solution and then glutaraldehyde (GA) cross-linked utilizing for beads preparation technique. Then the capability of these materials to remove heavy metals such as Mn^{2+}, Cu^{2+}, Fe^{3+}, Pb^{2+}, Zn^{2+}, Cd^{2+}, Ni^{2+}, Li^{2+}, Sr^{2+} and Al^{3+} from aqueous solution was considered. Through testing different adsorption mechanisms and kinetics models to appropriate our testing data, we also examined the adsorption kinetics and isotherms of some metal ions adsorption for Zeo/PVA/SA NC beads. The effect of the concentration of ZeoNPs into the PVA/SA, on the adsorption ability was also considered. The optimal preparation circumstances at which blending procedure continues homogeneously and extensively as pH, contact time, adsorbent dose, initial concentration of heavy meat ions and adsorption temperature on the elimination efficiency were studied. The characterization of SA, PVA/SA and Zeo/PVA/SA NC beads were studied via FTIR, SEM. The prospective use of synthesized beads in water treatment was examined. The reusability of the Zeo/PVA/SA NC beads was also examined. Consequently, the applicability of the synthesized Zeo/PVA/SA NC beads was indicated using groundwater samples collected from 10th Ramadan City, Cairo, Egypt to display the novelty of the selected beads for treatment of such polluted groundwater samples. Moreover, the antibacterial performance of the synthesized Zeo/PVA/SA NC beads was revealed via E. coli as an example of microorganisms in wastewater treatment. Presently, there are not stated articles occupied with the method Zeo/PVA/SA NC beads for removal of some heavy metal ions containing in the existing contribution.

2. Experimental

2.1. Materials and analytical method

All the reagents and chemical ingredients were used for analytical evaluation and were gotten from Sigma–Aldrich. Stock solutions of 1000 mg/L of Mn^{2+}, Cu^{2+}, Fe^{3+}, Pb^{2+}, Zn^{2+}, Cd^{2+}, Ni^{2+}, Li^{2+}, Sr^{2+}, and Al^{3+} were synthesized via dissolving dried quantities of anhydrous $MnCl_2$, $CuSO_4$, $FeSO_4$, $PbCl_2$, $ZnCl_2$, $Cd(CH_3COO)_2$, $NiCl_2$, $LiCl_2$, $Sr(NO_3)_2$ and Al_2O_3 salts, respectively, in distilled water, to attain standard solutions of 1000 ppm in every flask. Various concentrations of heavy elements were synthesized via diluting the standard solution. Solutions of 0.1 M sodium hydroxide (NaOH, 98%) or HCl (30%) were utilized for pH modifications via pH Meter (3510, Jenway, UK) and were purchased from El-Motaheda company. The adsorbed solutions were filtrated and directly analyzed via Inductively Coupled Argon Plasma-Mass Spectrometry (ICP-MS) 6500 Duo, (POEMS III); Thermo Jarrell Ash, USA. Sodium alginate (SA) was used as a polymeric substrate; it was supplied from BDH laboratory ingredients, England. Polyvinyl alcohol, (PVA, the quantity of hydrolysis: 87%) was supplied from Sigma–Aldrich. Glutaraldehyde (GA) aqueous solution was used as a cross-linking agent for SA/PVA composites was purchased from El Nasar Pharmaceutical Chemical Co. (ADWIC) Adowic Co. Acetone was used for GA preparation and was gotten from Sigma–Aldrich. Natural zeolite (Zeo) sample was gotten from RaaTec-Zeolite supplements Company with the chemical composition of Silicon oxide 1%, zeolite ssz-73 2.6%, Clinoptiloloite 81.1% and Donpeacorite 15.3%. The additional chemical, for example, inorganic salts, solvents other reagents, and organic compounds were component evaluation and used without extra purification.

2.2. Sample collection and analysis

The polluted samples were gathered from different locations in the 10th of Ramadan City, East El Delta, Egypt. The polluted samples were collected in a clean polyethylene bottle and used to determine the physical and chemical possessions of polluted water samples. The various field measurements were detected such as physical possessions through calculating the particular electrical conductance (EC) using EC meter pattern LF 538, WTW, USA and stated in micromhos for each centimeter (μmhos/cm) at 25 °C, and pH value was estimated using 3320 pH meter (Jenway, UK). The chemical investigates of the collected water samples was achieved at the central research laboratory of the Desert Research Center (DRC) in Cairo, Egypt. The collected samples were conserved and examined in the laboratory for major ions (Mg^{2+}, Ca^{2+}, K^+, Na^+, HCO_3^-, CO_3^-, SO_4^{2-}, Cl^-) utilizing standard approaches suggested via Rainwater and Thatcher, 1960; Fishman and Friedman, 1985 and APHA, 1995. The gotten chemical data are expressed in milligram per liter (mg/L) or part per million (ppm). The total dissolved solids (TDS in mg/L) were assessed by the following equation, where the TDS = Ca^{2+} + Mg^{2+} + Na^+ + K^+ + Cl^- + SO_4^{2-} + 0.5 (CO_3^{2-} + HCO_3^-), [Hem, 1991]. To determine the heavy metals 100 ml polyethylene bottle, followed by in situ acidification by nitric acid, conveyed to the laboratory in the icebox and stored at 4°C till

examination for heavy metal content. The samples were analyzed for Al^{3+}, Li^{2+}, B^{3+}, Co^{2+}, Fe^{3+}, Ni^{2+}, Sr^{2+}, Cd^{2+}, Cu^{2+}, Cr^{3+}, Zn^{2+}, Mn^{2+}, Pb^{2+}, and V^{2+} were achieved by Inductively Coupled Argon Plasma-Mass Spectrometry (ICP-MS) 6500 Duo, (POEMS III); Thermo Jarrell Ash, USA and 1000 mg/L (Merck) stock solution for stock production.

3. Methods and instruments

3.1. Preparation and characterization of zeolite nanoparticles (Zeo NPs)

The zeolite (Zeo) samples were grounded and sieved through a 1 mm sieve. The size of zeolite samples decreased to nano-level by a 24 blade FRITSCH Rotar Mortar (Model-Pulverizette-14). This method sustained for six steps. Subsequently, the grinded zeolite sample was burned at 400 °C for 2–3 h. The synthesized Zeolite nanoparticles (Zeo NPs) were stored to use for the modification of PVA/SA beads. The produced Zeo NPs were characterized via the examination of Fourier transform infrared spectrophotometry (FTIR) was achieved via a Genesis Unicam spectrophotometer, X-ray diffraction (XRD) were verified by (Philips pattern PW 3710), Particle size expansions via NICOMP Nano, PSS Particle sizing configurations Santa Barbara, California, USA, CW388 functionality form 1.71 and scanning electron microscopy (SEM). Around 0.1 mg of Zeo NPs was dispersed in 10 ml of deionized (DI) water and sonicated to 30 min. The Zeo NPs were distributed in DI water and the size dimensions were achieved at room temperature 25 °C at 90°/173° scattering angle.

3.2. Functionalization of nanocomposite beads

2 g of sodium alginate (SA) and 1 g Polyvinyl alcohol, (PVA) was dissolved in DI water and stirred at 80 °C for 2 h, Fig. 1. Afterward, various amount of Zeolite NPs (0.025–0.3 wt% based on the total amount of PVA/SA) were sonicated in an ultrasonic bath at 30 °C for 30 min to let Zeo NPs distributed in the deionized water, then mixed with the PVA/SA mixture for 1 h at 80 °C under vigorous stirring. The glutaraldehyde (GA) the cross-linking agent consists of 75 wt% (2% GA, 2% HCl and 71% acetone): 25 wt% DI water. The resulting mixture solution was poured as dropwise on a conical flask containing a GA cross-linking the solution, see Fig. 1. The resulting beads were left to solidify in this solution for 24 h and then subsequently washed with DI water until pH reached to 7 then it stored in deionized water. The resulting Zeolite/Polyvinyl alcohol/sodium alginate NC beads (Zeo/PVA/SA NCs beads) washed regularly with distilled water and saved in distilled water for performances and characterization. The SA and PVA/SA beads were prepared by the same previous method.

3.3. Adsorption experiments

3.3.1. Batch adsorption tests

The stock slandered solutions of 1000 mg/L of Mn^{2+}, Cu^{2+}, Fe^{3+}, Pb^{2+}, Zn^{2+}, Cd^{2+}, Ni^{2+}, Li^{2+}, Sr^{2+} and Al^{3+} were synthesized via dissolving a suitable quantity of the above metal ions salts in 1000 ml of DI water. Various concentrations (10, 30, 50, 70, and 100 mg/L) were prepared via dilution of the standard solution by DI H_2O. Batch adsorption tests were achieved on an automated shaker with a shaking rapidity of 150–200 rpm. To adjust the concentration of the adsorbent, various quantities of SA, PVA/SA and Zeo/PVA/SA NCs beads with Zeolite NPs 0.2 wt%, (0.5, 1, 2, 5, 10, 15 and 20 g/L) were joined to 50 ml of 25 mg/L of the above metal ions solution under mechanical shaking. To attain the influence of the pH standards of the above metal ion prepared solutions were adjusted by 0.1 M of both HCl and NaOH solutions. To achieve the influence of adsorption time, 1 g of SA, PVA/SA and Zeo/PVA/SA NCs beads was shacked with 50 ml of 25 mg/L of the prepared metal ion solutions at interval times (0, 15, 30, 45, 60, 75, 90, 105 and 120 min). To examine the impact of the temperature on the adsorbate solution, 1 g of adsorbent was shacked with 50 ml of 25 mg/L metal ion solutions at 25, 40 and 70 °C. Adsorption processes were achieved in 100 ml glass bottles placed in a shaker at a fixed speed 180 rpm until the equilibrium was touched. The various influences affecting adsorption techniques were considered.

The capacity of metal ions adsorbed was considered through the variance in the concentration of element ions in solution formerly and later the adsorption test and associated with the weight of the NC beads and expressed as mg/g. All the

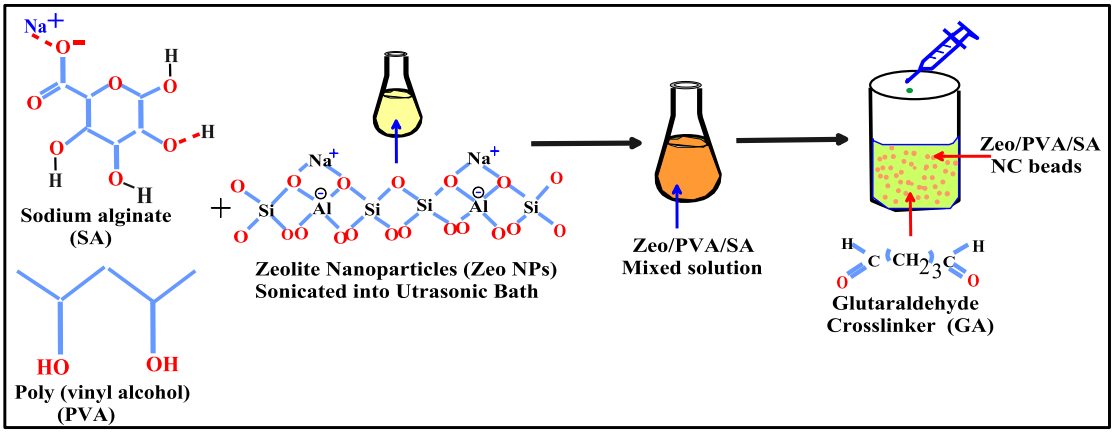

Fig. 1 Schematic representation of SA, PVA/SA and Zeo/PVA/SA NC beads.

tests were achieved three times and the average of three was occupied for successive calculations. The adsorption capability of synthesized beads was determined using the subsequent expression:

$$\mathbf{q_t} = [(\mathbf{C_0} - \mathbf{C_t})\ \mathbf{V}]\ /\ \mathbf{m} \quad (1)$$

The removal % of various metal ions was calculated via the following equation:

$$\% = (\mathbf{C_0} - \mathbf{C_t})\ /\mathbf{C_0 X\ 100} \quad (2)$$

where q_t is the number of metal ions adsorbed on the unit mass of the adsorbent Zeo/PVA/SA NCs beads (mg/g), C_0 and C_t are the initial concentration and the final element ion concentration after adsorption for t min. (mg/L), V is the volume of the adsorbate solution (L) and m is the mass of the adsorbent Zeo/PVA/SA NCs beads (g), respectively.

3.3.2. Desorption of metal ions and Reusability of chelating beads

Reusability of the prepared beads was achieved via washing with 0.1 M HCl solution with continuous shaking at 180 rpm for 1 h at 25 °C and formerly washed with DI H_2O numerous times and exposed to again to adsorption and desorption procedures several ten repeating cycles.

3.3.3. Antibacterial assessment of the synthesized beads

Pre-cultures of Escherichia coli (E. coli) cells were synthesized in 10 ml of Luria-Bertani (LB) standard (1 wt% yeast and 1 wt % sodium chloride in DI water) at 37 °C for 24 h. The synthesized media was diluted with DI water, and a dilute media (20 ml, total 350 cells) was pipetted onto the synthesized SA, PVA/SA and Zeo/PVA/SA NCs beads for 120 min. A volume of 1 ml of E. coli media was located on the LB agar medium and incubated for 24 h. The survival ratio of E. coli (%) was estimated by counting the integer of viable cells in expressions of colony-forming units (CFU/ml).

3.3.4. Application of the collected water samples using Zeo/PVA/SA NC beads

A 50 ml of the collected polluted samples were equilibrated with 1 g of the synthesized Zeo/PVA/SA NCs beads for 24 h at 25 °C and then the residual solution was re-tested.

4. Result and discussion

4.1. Characterization of the synthesized Zeo NPs

4.1.1. FTIR of the synthesized Zeo NPs

The functional groups of the prepared Zeo NPs were examined via the FTIR spectrum. Fig. 2a displays the spectra of Zeo NPs in the range of 400–4000 cm^{-1}, at 25 °C, FTIR analysis shows that Zeo NPs are considerably hydrated which is described by detached water absorption bands in the 1631 cm^{-1} region, which related to interstitial bonded water. This band refers to the water molecule associated with Na and Ca in the canals and cages of the zeolite structure. The band near 3610 cm^{-1} which indicates the —OH groups represent inter and intermolecular hydrogen bonding between octahedral and tetrahedral zeolite structure. A stretching band of Si—O nearby 1032 cm^{-1} was displayed. The peak confined at 1023 and 538 cm^{-1} relates to the vibration of the bands associated with the interior Si—O(Si) and Si—O(Al) vibrations in tetrahedral or silico– and alumino-oxygen bonds, respectively [Castaldi et al., 2008]. The peak localized at 457 cm^{-1} corresponds to Si—O—Si bending. The band appears around 789 cm^{-1} which exposes the NaO.

4.1.2. X-ray diffraction patterns of the synthesized Zeo NPs

The prepared Zeo NPs were described via X-ray deviation and showed crystalline structures. As displayed in Fig. 2b there were fifteen obvious pure diffraction peaks at 2θ equal to 12.4°, 14.8°, 15.5°, 19.0°, 20.1°, 23.4°, 24°, 25.7°, 27.5°, 28.6°, 29.2°, 31.0°, 33.8°, 41.4°, and 48.6°, respectively. These peaks confirmed by the standard data sheets for zeolite (ref's: 00-045-0437 and 01-076-0591) indicated by the Joint Committee on powder diversion, which approves the formation of zeolite NPs [Shalaby et al., 2018]. The medium particle size for the Zeolite nanoparticles was assumed by Scherer's equation:

$$\mathbf{d} = \frac{0.9\lambda}{\beta \mathbf{COS}\theta} \quad (3)$$

where λ is the wavelength of the X-ray (1.54 A°), d is the crystallite diameter of Zeo NPs, β is the whole width at half maximum width of the diffraction peak in radiance, and θ is the maximum intensity of the diffraction angle. The medium crystallite size of Zeo NPs was determined to be between 68 and 117.8 nm, with an average size of 87 nm. The X-ray diffusion patterns of all examined constituents displayed a great grade of crystallinity.

4.1.3. The particle size distribution (PSD) of the synthesized Zeo NPs

Fig. 2c displays a histogram of the results gotten from the dimensions of the particle size distribution (PSD) of Zeo NPs. The mean diameter and standard deviation values of the Zeo NPs size were 109.9 nm and 65.9 nm (60%).

4.1.4. Morphology analysis of the synthesized Zeo NPs

The surface images of the Zeo NPs were described via scanning electron microscopy (SEM). In Fig. 2d the Zeo NPs with different magnification were looked in asymmetrical shapes like, with smooth exteriors and a size variety around 80–120 nm with an average of 95 nm. The size variety obtainable here is near to the earlier dimensions gotten from both X-ray and particle size distribution. Additionally, the chemical reactivity of the nanoparticles resorts to be improved because of reducing particle size owing to an improvement in the surface to volume proportion.

4.2. Beads characterization

4.2.1. FTIR spectroscopy

FTIR spectroscopy can provide an effective and appropriate technique to conclude the functional groups of the neat cross-linked SA, PVA/SA, Zeo/PVA/SA and after Cu^{2+} ions adsorption, Cu/Zeo/PVA/SA NC beads which illustrated in Fig. 3. FTIR was achieved to confirm the effective blending of PVA and Zeo NPs onto the SA mixture resulting in Zeo/PVA/SA NC modified beads. The FTIR spectra of the neat SA structured beads indicate the presence of peaks at 2931

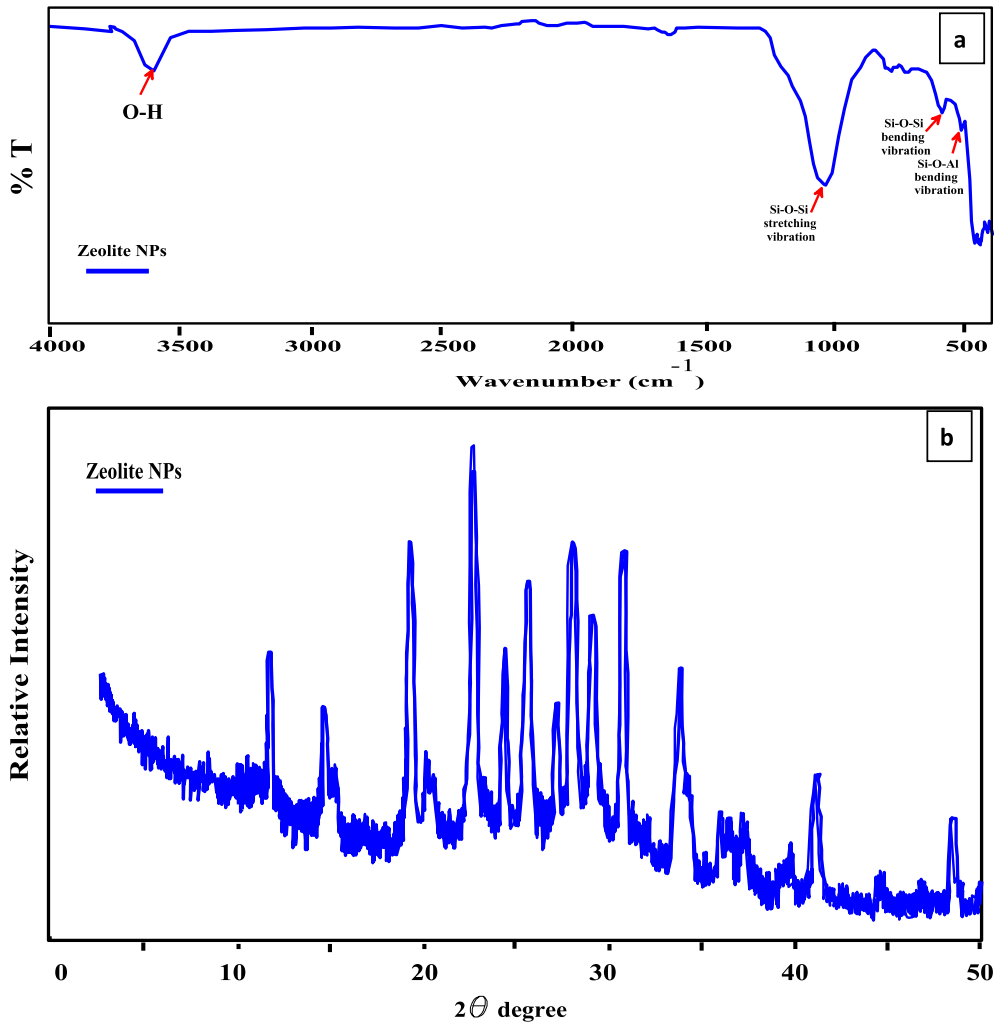

Fig. 2 (a) FTIR spectra of prepared Zeo NPs; (b) X-ray diffraction pattern of prepared Zeo NPs; (c) Histogram of Zeo NPs Particle size spreading and (d, e, f, g and h) SEM images of Zeo NPs.

and 1090 cm^{-1} were attributed to C—H stretching bond and C—O— groups, respectively. A broad and strong band appeared at 3395 cm^{-1} related to the —OH stretching vibrations of the hydroxyl group, while the band around 1616 cm^{-1} might be related to C═O stretching of the carbonyl group and/or was owed to the vibration of adsorbed H_2O on neat SA beads. The bands appear around 1025 and 1733 cm^{-1} attributed to the C—O—C stretching bond and C═O stretching bond of the cross-linked SA. The presence of three bands around 1225, 948 and 789 cm^{-1} which related to the C—C stretching bond, C—O attributed to its saccharine structure and Na—O characteristic peak of SA. The symmetric band appears around 1405 cm^{-1} which belongs to O—C═O group. Comparing the FTIR band of PVA/SA and Zeo/PVA/SA, we can find that the typical bands revealed above of the later are distantly affected in their intensity and position. The FTIR band of PVA/SA in Fig. 3 displays that the O—H stretching vibration band at 3366 cm^{-1} and O-H bending at 1120 cm^{-1} moved to lower wavenumbers owing to the interaction of hydroxyls between PVA and alginate [Chen et al., 2010]. The C═O stretching vibration at 1410 and 1636 cm^{-1} also moved to a higher value, proposing the probability of ionic bonding formed between the cross-linker and COO— groups [Hua et al., 2010]. The peak around 1400 cm^{-1} was owed to C—OH.

The FTIR of the Zeo/PVA/SA NC beads show a wide band around 3364 cm^{-1} was due to —OH stretching and the peak intensities enlarged according to the amount of Zeo NPs inside the beads. This could be owed to the hydrophilic nature of Zeo NPs which can adsorb water molecules via H–bonding. The appearance of a new band at about 538 and 960 cm^{-1} which is attributed to Si—O—Al and Si—O—Si bonds of Zeolite NPs, respectively [Yurekli 2016]. The peak localized at 457 cm^{-1} corresponds to Si—O—Si bending. The occurrence of several oxygenous functional groups showed that Zeo NPs were effectively reacted. The plentiful oxygenous functional groups create Zeo/PVA/SA NC beads strongly hydrophilic, which improves their solubility in water.

Comparing the FTIR spectrum of the Zeo/PVA/SA NC beads before and after Cu^{2+} ions adsorption, we can find that the position and the intensity of the peaks shifted after adsorption of Cu^{2+}, which can be seen in Fig. 3. The FTIR spectrum of Zeo/PVA/SA NC beads after Cu^{2+} ions adsorption in Fig. 3 displays that the O—H stretching vibrations at

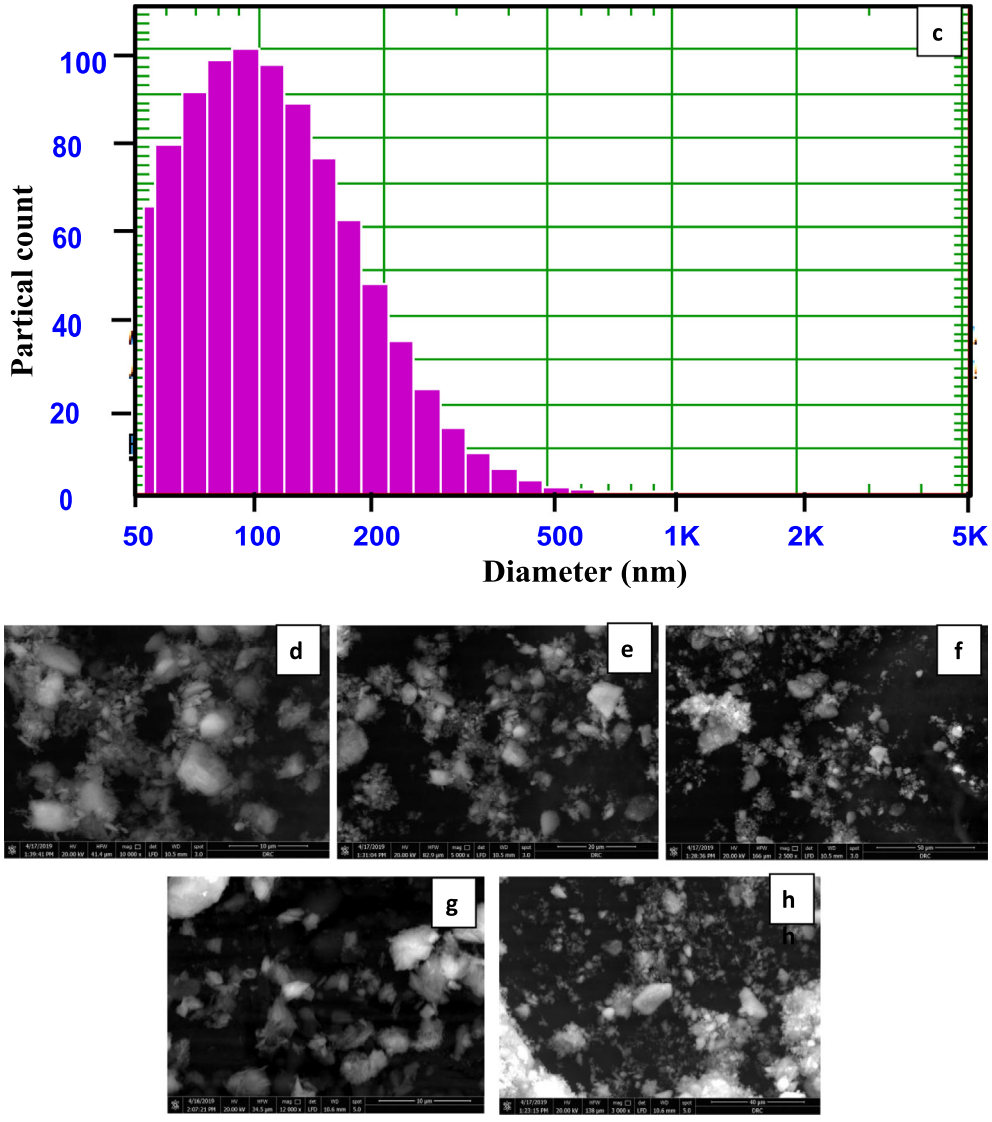

Fig. 2 (*continued*)

3273 cm^{-1} moved to lower wavenumbers owing to the adsorption of Cu^{2+} ions on the surface of Zeo/PVA/SA NC beads. The complex of Cu^{2+} displays strong and abroad band in region 3273 cm^{-1} attributed to vibration band of O-H stretching vibrations of coordinated H_2O molecules [Sandra et al., 2007]. This interaction might be due to the physical method that might be via weak electrostatic interaction or via complexion and Vander Waals forces [Rafatullah et al., 2009]. The FTIR bands of adsorbed Cu^{2+} ions using Zeo/PVA/SA NC beads shows elongation of these bands after Cu^{2+} ions adsorption representing the mode of these group in adsorption procedure. The outcomes indicated that alkynyl, hydroxyl, and alkoxy groups participated in the adsorption process and provided unshared pair electrons played an important effect on the adsorption of Cu^{2+} ions. Compared with the bands of the original PVA/SA/Zeo, the carboxylic group appear at 1576 cm^{-1} after Cu^{2+} adsorption were got longer to a certain range of about 1586 cm^{-1} than those before adsorption. This outcome showed that the adsorption could have generally happened through the interaction among divalent cations Cu^{2+} and the —COO and O—H groups and/or the ions exchange and the adsorption behavior was mostly ruled via chemical adsorption. The band appears at 1697 and 1339 cm^{-1} related to the asymmetric and symmetric vibrations of the carboxylic group of the metal restrictive carboxylates which is related to monodentate coordination of both the carboxylate groups [Olmez et al., 2004]. The band of complex Cu^{2+} around 460 cm^{-1} effects from vibration band of Cu—O stretching vibration [Nakamoto 2006] which is attributed to the reaction of the Cu^{2+} with surface OH groups. This is an indication of complex formation between Cu^{2+} ions and anionic species. Based on the changes in the FTIR spectra, it can be assumed that Hydroxyl and carboxyl groups might be functional groups involved in the adsorption of Cu^{2+} ions. The position of the peaks shifted after adsorption of Cu^{2+} ions, these results point to the —OH, —COO, —C—O—C—, —C≡C—, Si—O—Al, Si—O—Si bonds groups contributed in the adsorption procedure and given that unshared pair electrons played a

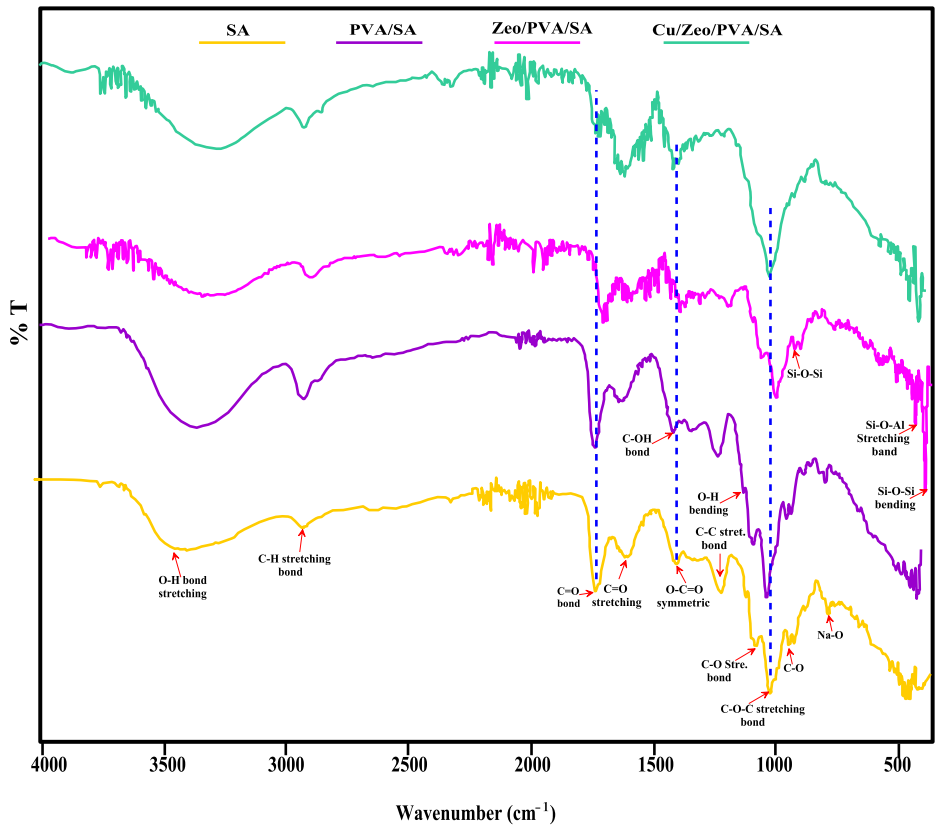

Fig. 3 FTIR spectra of SA, PVA/SA, Zeo/PVA/SA and after Cu^{2+} ions adsorption Cu/Zeo/PVA/SA NC modified beads.

significant influence on the adsorption of element ions. The disappearing Na—O bond after adsorption of Cu^{2+} may be due to the cation exchange process. The appearance of a new band at 490 cm^{-1} is due to Cu^{2+} complex.

4.2.2. Morphology analysis of beads

The SEM images with the different magnification of the surface and inner structures of SA, PVA/SA, Zeo/PVA/SA and after Cu^{2+} ions adsorption Cu/Ceo/PVA/SA NC modified beads are revealed in Fig. 4. As revealed in Fig. 4, the surface of the neat cross-linked SA was relatively smooth. Fig. 4 indicates that the PVA/SA beads had a rough and ridged surface with many folds and creases with increasing the pores existing in the inner structure of the beads. Fig. 4 indicates that the Zeo/PVA/SA NC beads showed rougher, loose surfaces with porous structure and the dispersion of Zeo NPs clustering that contains lots of tiny interspace structure with a small number of dimples and bumps and an irregular inner morphology. After the incorporation of Zeo NPs, the inner structure of the beads was irregular and rough with increasing the microporous structure as well as, the cavities and pore opening have been shown in Fig. 4 which improves the adsorption process which might increase contact surface area between adsorbent and the modified NC beads, and provide more active sites, thus improving their adsorption performances Fig. 4. The active sits and pores allow water to pass through it then the cation exchange may be occurring. The Zeo NPs enhance the mechanical possessions and increases the surface area of the synthesized beads which means that the adsorption will be very easy and very fast Fig. 4. SEM images of Cu/Zeo/PVA/SA NC beads that have absorbed Cu^{2+}, the differences are more observable, the surface of Zeo/PVA/SA NC beads drastically changed after Cu^{2+} adsorption. It can be indicated that the pore and the cavities become rough along with irregular form and cracks, this mainly owing to the physical and the chemical damage throughout the adsorption process of the metallic ions [Zamzow et al., 1990]. SEM images confirm that Cu^{2+} ions were absorbed and dispersed homogeneously all over the whole mass of the beads and suggesting that all reactive groups contributed in the reaction at an optimum time that has been allowed Cu^{2+} ions to migrate from the aqueous solution to be sorbent into Zeo/PVA/SA NC beads as showed in the photographed image Fig. 4. Fig. 4 revealed that the color of PVA/SA and Zeo/PVA/SA and after Cu^{2+} ions adsorption Cu/Zeo/PVA/SA as well as showed the absorbed Cu^{2+} inside the tissue of the Zeo/PVA/SA NC beads.

Additionally, Zeo/PVA/SA NC beads had a like pore structure but observably had much more pores when compared to originator PVA/SA, which should be owing to the surface modification procedure and the presence of Zeo NPs. These micro and nano-pore are responsible for the water-induced phase separation through the metal removal process. The porous structure would allow the adsorption happening on both exterior and interior of adsorbents, subsequently simplifying the metal ions adsorption nevertheless wanting superior contact time for equilibrium and (soaking) saturation. After the adsorption, the Zeo/PVA/SA NC beads continued porous structures due to relatively large pores. Meanwhile, Zeo/PVA/SA NC beads result in Fig. 4 confirmed the presence of Cu^{2+} onto the Zeo/PVA/SA NC beads, suggesting Cu^{2+}

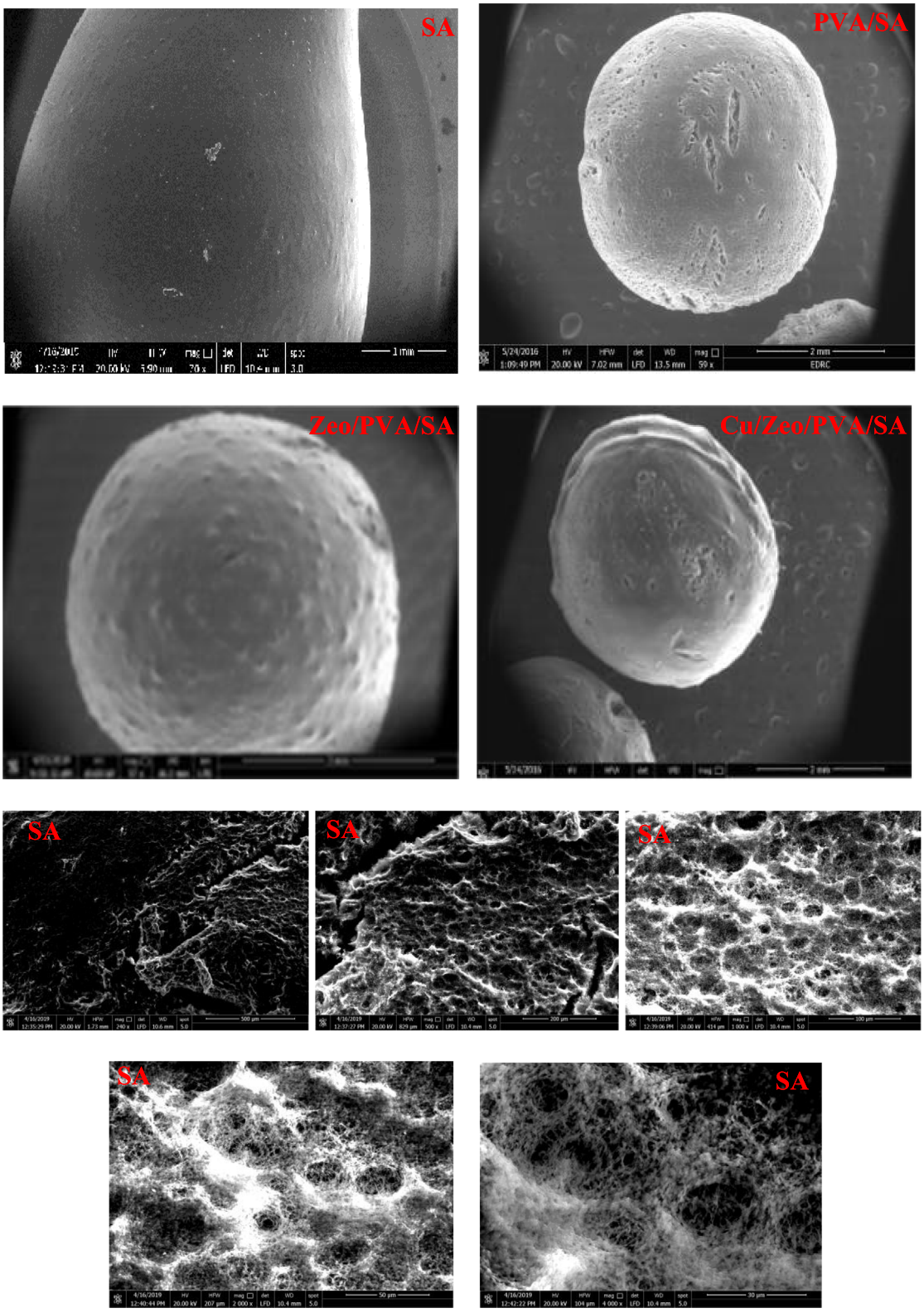

Fig. 4 SEM images at different magnifications for the surfaces and cross section of SA, PVA/SA, Zeo/PVA/SA and after Cu^{2+} ions adsorption Cu/Zeo/PVA/SA NC modified beads and the photograph images of PVA/SA, Zeo/PVA/SA and after Cu^{2+} ions adsorption Cu/Zeo/PVA/SA NC modified beads.

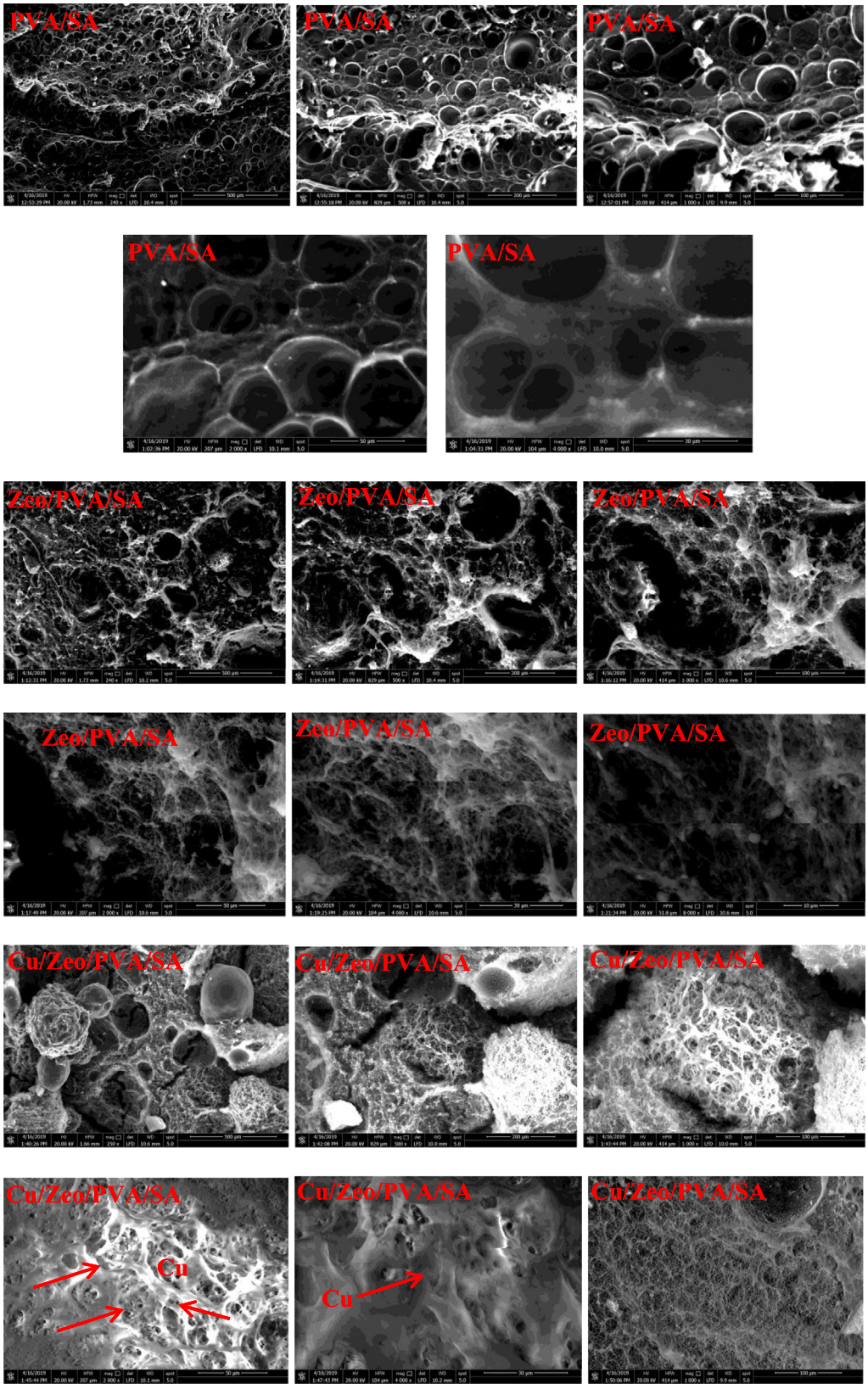

Fig. 4 (*continued*)

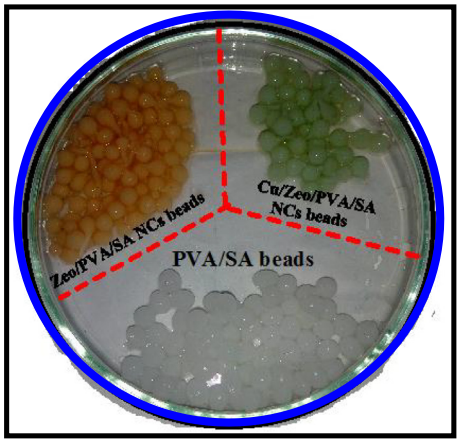

Fig. 4 (*continued*)

was adsorbed on the adsorbent successfully. Furthermore, the disappearing of Na (I) ions inferred that the adsorption mechanism included ion exchange as confirmed through the FTIR studying.

4.3. Adsorption experiments of the synthesized beads

4.3.1. Effect of the adsorbent chemical composition

In the existent work, the removal efficiency (%) of the metal ions mostly attributed to the amount of the active spots and chemical structure of the adsorbent. The use of binary comonomer structure is an attitude to improve the functionality of the prepared beads by presenting two function groups of numerous chemical behavior and nature. The existence of further than one monomer may result in the hindering or the improvement of the removal efficiency. The removal efficiency of the PVA/SA binary structure of various comparative compositions (0/1, 1:1, 1:2, and 2:1 wt%) examined and displayed in Fig. 5. The results illustrate that the use of PVA/SA (1:2 wt %) indicated that the higher removal efficiency when compared to the other comonomer compositions. Fig. 5 displays that the use of a comonomer solution rich in SA leads to a higher removal efficiency of the metal ions as compared to that synthesized via PVA rich comonomer, so, the increment in the PVA content in the comonomer solution decreased the removal efficiency of the metal ions. It can be found that the order of metal ions removal is PVA/SA (1:2) > PVA/SA (2:1) > PVA/SA (1:1) > PVA/SA (1:0). This increase in the removal efficiency is mainly owing to the improving number of active spots and potential spots [Idris et al., 2012] and the presence of the reactive groups of PVA, in addition to the chelation effect of SA with metal ions. The incorporation of PVA enhances the mechanical possessions of the synthesized beads. These outcomes could expose the high capacity of the PVA for homo-polymerization and crosslinking through the transformation of monomer molecules into the polymer. Such homo-polymerization indications that the increase in the reaction medium viscosity and subsequently to control the movement of the free radical to reach the active spots on the polymeric substrate, causing in decreasing the elimination efficiency of the metal ions obtained. Furthermore, the hydroxyl groups in SA also own the ability for cation exchange, therefore improved the metal ions adsorption efficiency [Bée et al., 2011]. The obtainability of ion exchangeable spots and active sites for metal ions were importantly improved owing to the increase SA dosage. Consequently, the adsorption efficiency of PVA/SA beads improved with the increased dosage of SA content.

4.3.2. Effect of zeolite NPs concentrations

The removal efficiency of various metal ions could be affected via the Zeo NPs dosage incorporated in PVA/SA mixture solution. Fig. 6 shows the effect of Zeo NPs amount on the removal efficiency the selected metal ions (Al^{3+}, Li^{2+}, Fe^{3+}, Ni^{2+}, Sr^{2+}, Cd^{2+}, Cu^{2+}, Zn^{2+}, Mn^{2+}, and Pb^{2+}) in the range from 0.025 to 0.3 wt% related to SA/PVA concentration, (i.e. 3 wt%) for the initial metal ions concentration 25 mg/L at 25 °C and at the ambient pH (2–8) according to

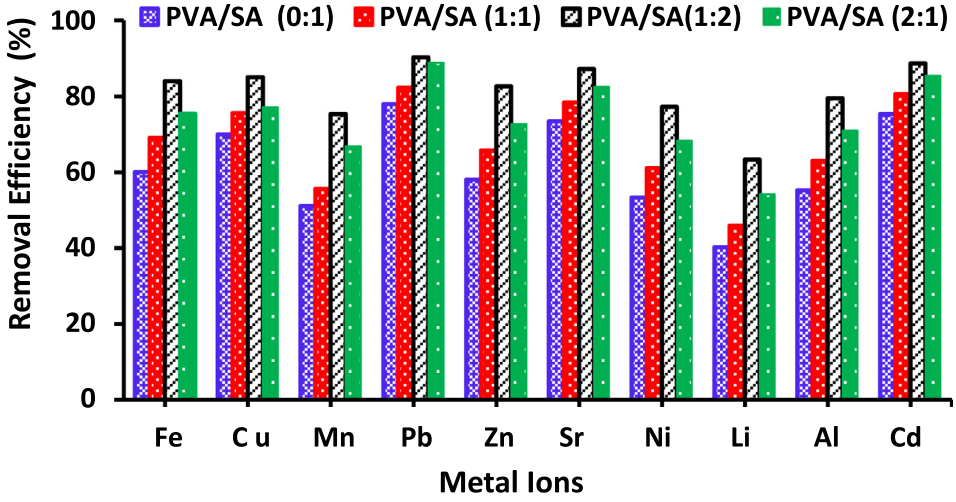

Fig. 5 The effect of PVA/SA binary comonomer concentration on the removal efficiency of the selected metal ions (Al^{3+}, Li^{2+}, Fe^{3+}, Ni^{2+}, Sr^{2+}, Cd^{2+}, Cu^{2+}, Zn^{2+}, $Mn^{2+}$and Pb^{2+}), metal ions concentration = 25 mg/L, pH = 3–8, t = 24 h, adsorbent dose is 20 g/L, Zeo NPs concentration = (0.2 wt%) at 25 °C.

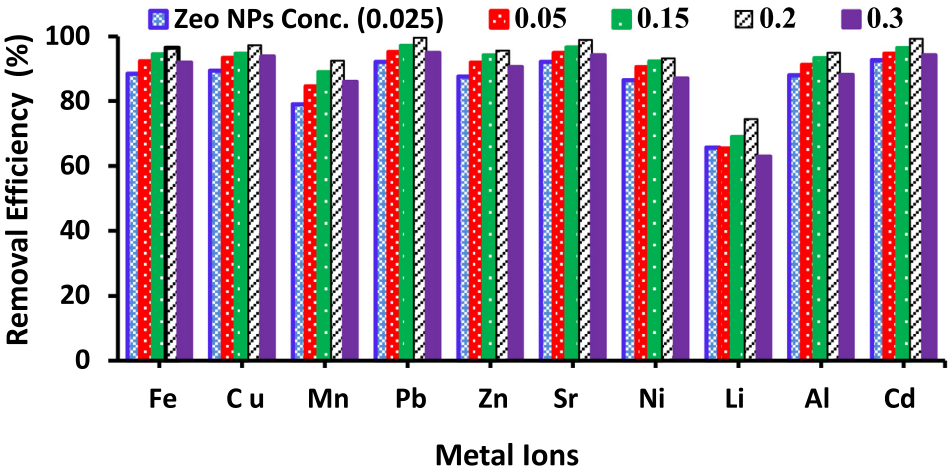

Fig. 6 The effect of Zeolite NPs concentrations on the removal efficiency of the selected metal ions (Al^{3+}, Li^{2+}, Fe^{3+}, Ni^{2+}, Sr^{2+}, Cd^{2+}, Cu^{2+}, Zn^{2+}, $Mn^{2+}$and Pb^{2+}), metal ions concentration = 25 mg/L, pH = 3–8, t = 24 h, adsorbent dose is 20 g/L, PVA/SA concentration (1:2 wt%) adsorbent dose is 20 g/L at 25 °C.

the type of the metal ions. It is found that 0.2 wt% of Zeo NPs are considered as the optimal dose at contacting time of 12 h. It is found that the elimination efficiency of the selected metal ions increases with increasing the Zeo NPs concentrations this is due to the improving the number of oxygen functional groups of Zeo NPs that are protonated by low pH values and increased the active sites for heavy metal ions chelation. The figure displays no further increase in the heavy meat ions removal as Zeo NPs dose increased rather than 0.2 wt%. Beyond a Zeo NPs concentration of 0.2 wt%, the removal efficiency decrease with increasing Zeo NPs concentrations. All Zeo structure is consists of an alumino-silicate [$Si(OH)_4$ and Al $(OH)_4$] framework which involves a crystalline tetrahedral organization of aluminum cations (Al^{3+}) and silicon cations (Si^{4+}) that are bounded by four oxygen anions (O^{2-}). These enrich oxygen functional groups are responsible for the higher elimination efficiency of the metal ions. The resulting negative locations are balanced via counter ions which are generally alkaline or alkaline earth metals, such as Na^+, K^+, Mg^{2+}, Ca^{2+} as well as can attach the heavy metal ions via cation exchange procedure [Moshoeshoe, 2017]. Zeo NPs have Cage–like structure containing channel (pore) size contingent upon the Si: Al ratio, the counter-cation active are responsible for the heavy metal ions removal.

4.3.3. Effect of temperature

It is fine identified that the temperature has a pronounced influence on every chemical procedure therefore it may improve or hinder such procedure depending on the environment of the reactants and/or the produces. The change in temperature is responsible for the improvement of the diffusion rate of the adsorbate molecule through the exterior boundary layer and inside the pores of the adsorbent [Chen et al., 2010]. Additionally, varying the temperature will improve the equilibrium ability of the adsorbent for a specific adsorbate. The influence of temperature on the adsorption of the selected metal ions (Al^{3+}, Li^{2+}, Fe^{3+}, Ni^{2+}, Sr^{2+}, Cd^{2+}, Cu^{2+}, Zn^{2+}, $Mn^{2+}$and Pb^{2+}) was achieved at 25, 40 and 70 °C using Zeo/PVA/SA NC beads. Fig. 7 revealed that the removal efficacy of the selected element ions from an aqueous solution is affected by the reaction temperature. The figure displays an unexpected effect as the metal adsorption declined unusually with increasing the adsorption temperature. The decrease in metal ions adsorption ability of the adsorbent with greater temperature showed the exothermic environment of the adsorption procedure. The decrease in (Al^{3+}, Li^{2+}, Fe^{3+}, Ni^{2+}, Sr^{2+}, Cd^{2+}, Cu^{2+}, Zn^{2+}, $Mn^{2+}$and Pb^{2+}) uptake with the greater temperature clarified from two features. Firstly, as the temperature increases, the diffusion of metal ions becomes much difficult in the Zeo/PVA/SA NC beads due to the decrease in the degree of swelling, therefore the adsorption capability of metal ions decrease too. Secondly, the bond split of the reactive groups on the adsorbent surface at a greater temperature may decrease the number of active adsorption spots, which might also cause a decrease in the adsorption amplitude of the adsorbent.

4.3.4. Effect of initial metal feed concentration

The initial element ion concentration of the solution shows an essential role as a driving force to restrain the mass transfer resistance between the solid phases and solution. The efficiency of the chelating sorbent at various effluence concentrations is also a good estimating thing for the synthesized Zeo/PVA/SA NCs beads. Fig. 8 displays the effect of metal ions concentration on the adsorption procedure after 24 h were the initial metal ions concentrations in the variety of 5–55 mg/L (adsorbent dose of 20 g/L; pH = 3–6 according to the type of metal ions; at 25 °C). Consequently, the number of element ions adsorbed was anticipated to be greater with a higher initial element ions concentration. Fig. 8 displays that, the removal efficiency was decreased with higher initial element ions concentration according to the type of metal ions. We can find that when the initial element ions concentration increased from 5 to 55 mg/L, the removal efficiency decreased according to the selected metal ions. This can be considered from two features. Firstly, a higher concentration of metal ions led to more binding locations on the surface of Zeo/PVA/SA NCs beads related to lower initial element ions concentration at the same dose of adsorbent [Barala et al., 2009] Secondly, higher initial element ions concentration improved driving force to control the mass

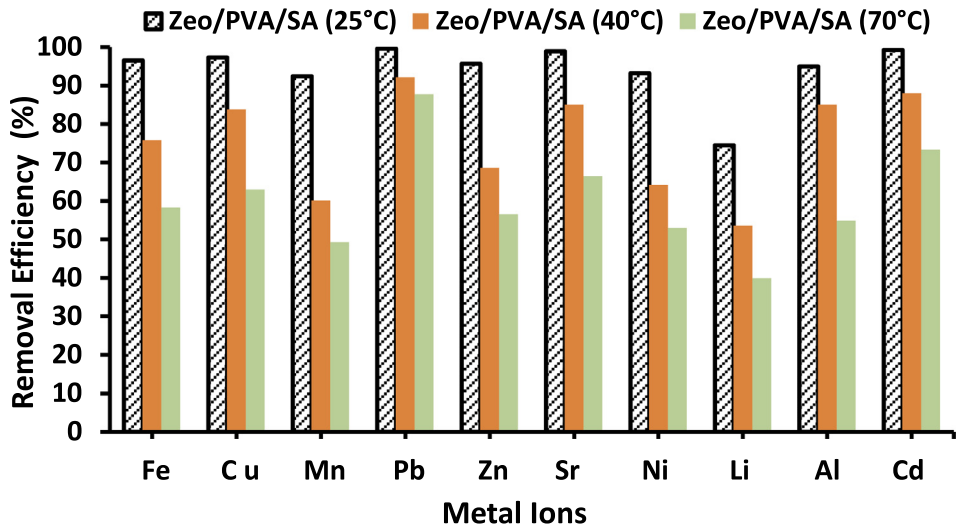

Fig. 7 Effect of temperature on adsorption of the selected metal ions (Al^{3+}, Li^{2+}, Fe^{3+}, Ni^{2+}, Sr^{2+}, Cd^{2+}, Cu^{2+}, Zn^{2+}, $Mn^{2+}$and Pb^{2+}), metal ions concentration = 25 mg/L, pH = 3–6 according the type of metal ions, adsorbent dose is 20 g/L, t = 24 h.

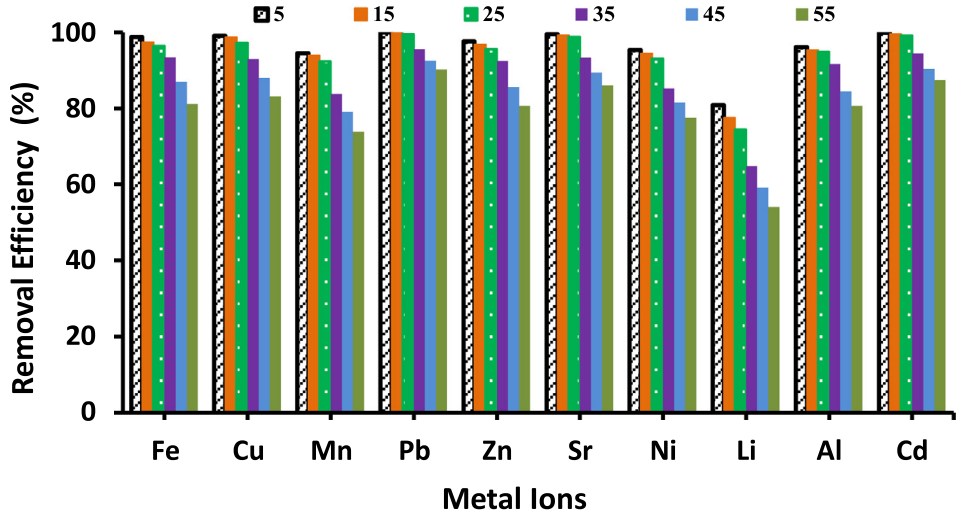

Fig. 8 The effect of individual metal ions concentration on their adsorption (Al^{3+}, Li^{2+}, Fe^{3+}, Ni^{2+}, Sr^{2+}, Cd^{2+}, Cu^{2+}, Zn^{2+}, $Mn^{2+}$and Pb^{2+}), metal ions concentration ranged from 5 to 55 mg/L, pH = 3–6 according the type of metal ions, adsorbent dose is 20 g/L, t = 24 h at room temperature (25 °C).

transference resistance of metal ions among the solid phases (beads) and aqueous causing a higher possibility of collision among the metal ions and Zeo/PVA/SA NCs beads as well as, the decrease of metal ions uptake the Zeo/PVA/SA NCs beads with increasing initial metal ions concentration may also be owing to a further intensity interaction between the metal ions and Zeo/PVA/SA NCs beads.

4.3.5. Effect of contacting time

The effects of contact time on the adsorption of the selected metal ions (Al^{3+}, Li^{2+}, Fe^{3+}, Ni^{2+}, Sr^{2+}, Cd^{2+}, Cu^{2+}, Zn^{2+}, $Mn^{2+}$and Pb^{2+}) are studied at interval time 0–120 min which revealed in Fig. 9. The contact time experiments were taking place at the adsorbent dose of 20 g/L, element ions concentration 25 mg/L, pH value of 3–6 according to the type of metal ions, at 25 °C. From Fig. 9, it has been revealed that the adsorptions of the selected ions from their aqueous solution are improving with increasing the contacting time. The increase in elimination efficiency with increasing the contact time is attributed to the point that further time becomes obtainable for metal ions to interaction with Zeo/PVA/SA NCs beads. It also displays that Zeo/PVA/SA NCs beads are very operative for removal of the under investigation metal ions. The removal efficiency is in order; Pb > Cd > Sr > Cu > Fe > Zn > Al > Ni > Mn > Li ions, respectively where the adsorption is fast within the first 70 min, then increase slowly and the adsorption procedure achieved equilibrium within 120 min. The initial metal ions adsorption rates by Zeo/PVA/SA NCs beads are very high as a bulky number of adsorption spots are obtainable for

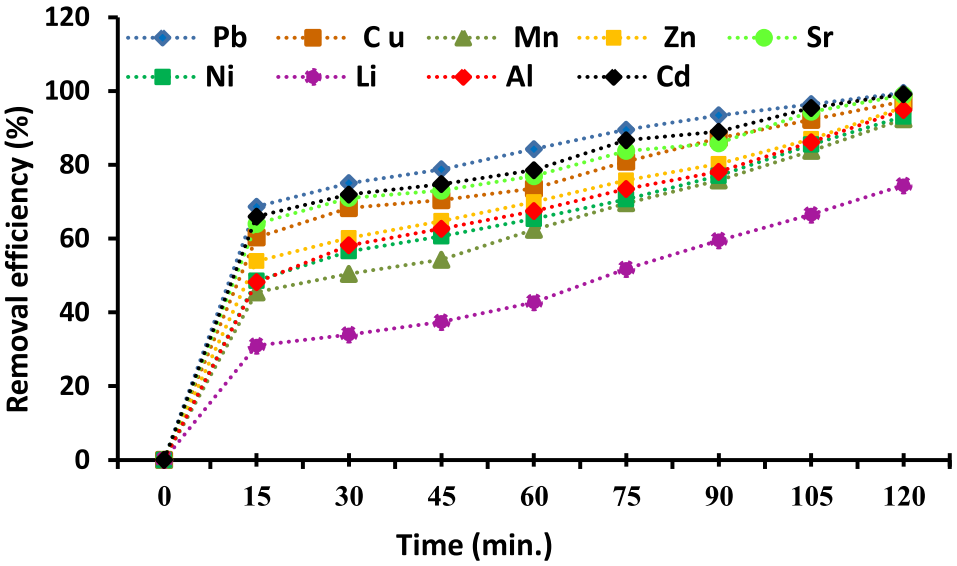

Fig. 9 The effect of contacting time on adsorption of Al^{3+}, Li^{2+}, Fe^{3+}, Ni^{2+}, Sr^{2+}, Cd^{2+}, Cu^{2+}, Zn^{2+}, $Mn^{2+}$and Pb^{2+}, Metal ions concentration 25 mg/L, Temp. = 25 °C, pH = 3–8, time ranged from 0 to 120 min., adsorbent dose is 20 g/L.

adsorption. Briefly, in the initial creative surface, the penetrating possibility is large and therefore adsorption procedures with a high level. When the accessible allowed surface is gradually occupied with the adsorbate sorts, adsorption procedure becomes slow and the kinetics may take place further reliant on the degree at which the adsorbate particles penetrate via the pores and become adsorbed onto the surface of the inside pores.

4.3.6. Effect of pH value of the solution on adsorption

The solution pH is an essential monitoring influence in the adsorption procedure as a result of its influence on the chemical speciation of the metal ions in sorbate and the ionization of chemically active spots (dissociation/association of the acidic groups and/or protonation/deprotonating of the basic groups) on the adsorbent surface [Petrovic et al., 2016]. The variation of selective metal ions adsorption by Zeo/PVA/SA NCs beads with pH may be attributed to the surface charges and the dispersed species of metal ions in solution to optimize the pH value for maximum elimination efficiency. The influence of pH on the adsorption amount of Al^{3+}, Li^{2+}, Fe^{3+}, Ni^{2+}, Sr^{2+}, Cd^{2+}, Cu^{2+}, Zn^{2+}, $Mn^{2+}$and Pb^{2+}on Zeo/SA/PVA NCs beads was examined after soaking the functionalized beads in aqueous heavy metal ions solutions for 24 h within pH varieties between 1.0 and 9.0, adsorbent dose of 20 g/L, the initial element ions concentration of 25 mg/l at 25 °C, as displayed in Fig. 10a. From Fig. 10a, we concluded that the removal efficiency reached maximum at the pH value of 6.0 for Pb^{2+}, Cd^{2+}, Sr^{2+}, Cu^{2+}, Zn^{2+}, Ni^{2+}, Mn^{2+} and Li^{2+} with 99.5, 99.2, 98.8, 97.2, 95.6, 93.1, 92.4 and 74.5%, respectively, while the highest removal are achieved at pH = 5 for Fe^{3+} and Al^{3+} with 96.5 and 94.9%, respectively and decreased at lower or higher pH values. These manners can be attributed to protonation and de-protonation of the functional groups of the adsorbent [Mousavi et al., 2010] as well as, the difference in the ionic state of the acid-reactive carboxyl groups in the adsorbent.

As it is revealed in Fig. 10b, the removal efficacy of the selective metal ions from the solutions slightly increased with increasing the pH from 1.0 to 5.0 using Zeo/PVA/SA NCs beads to reach the maximum adsorption value are achieved at pH = 6 for Pb^{2+}, Cd^{2+}, Sr^{2+}, Cu^{2+}, Zn^{2+}, Ni^{2+}, Mn^{2+}, and Li^{2+}, while the highest removal is attained at pH = 5 for Fe^{3+} and Al^{3+}. An additional increase of the pH from 5 and/or 6 to 9 according to the type of the metal ions the removal decreased. Slight sorption at lower pH could be attributed to the H^+ ions competing with metal ions for replaceable cations, on the surface of Zeo/PVA/SA NCs beads because of the high H^+ concentration. Furthermore, the reduction of the attraction among adsorbents and metal cations is mainly because of the positive charge of the sorbent's surface. In contrast, in the pH variety from 1.0 to 4.0, the deprotonation of COOH groups on the Zeo/PVA/SA NCs beads surface occurs, permitting superior adsorption of metal ions [Chen et al., 2010]. Meanwhile, metal ion species exist in acidic solution as bulky hydrated species, these ions was too big to enter in the micro-porous of the Zeo/PVA/SA NCs beads. In the pH variety from 4.0 to 6.0, a small increase of metal removal is observed that might be described by the fact that the adsorption spots are no more affected via the pH change. The detected data at low pH values (pH < 2) could be attributed to the electrostatic repulsion among the metal ions in the medium (M^+) and the positive charges accrued on the surface of the beads due to the protonation of the Zeo/PVA/SA NCs beads moieties. Such repulsion inhibits the approach of the metal ions to the surface of the beads [Kornicker and Morse 1991]. By increasing the pH value, such positive charge concentration declines to permit the metal ions to attitude the sorbent beads surface which causes greater removal efficiency. At a higher pH, the selective metal ions precipitate in the form of hydroxides ($M(OH)_2$) form which consequently reduces removal efficiency causing in a minimization of the adsorption values this decreases the rate of adsorption and subsequently the removal efficiency of metal ions Fig. 10b. This can also

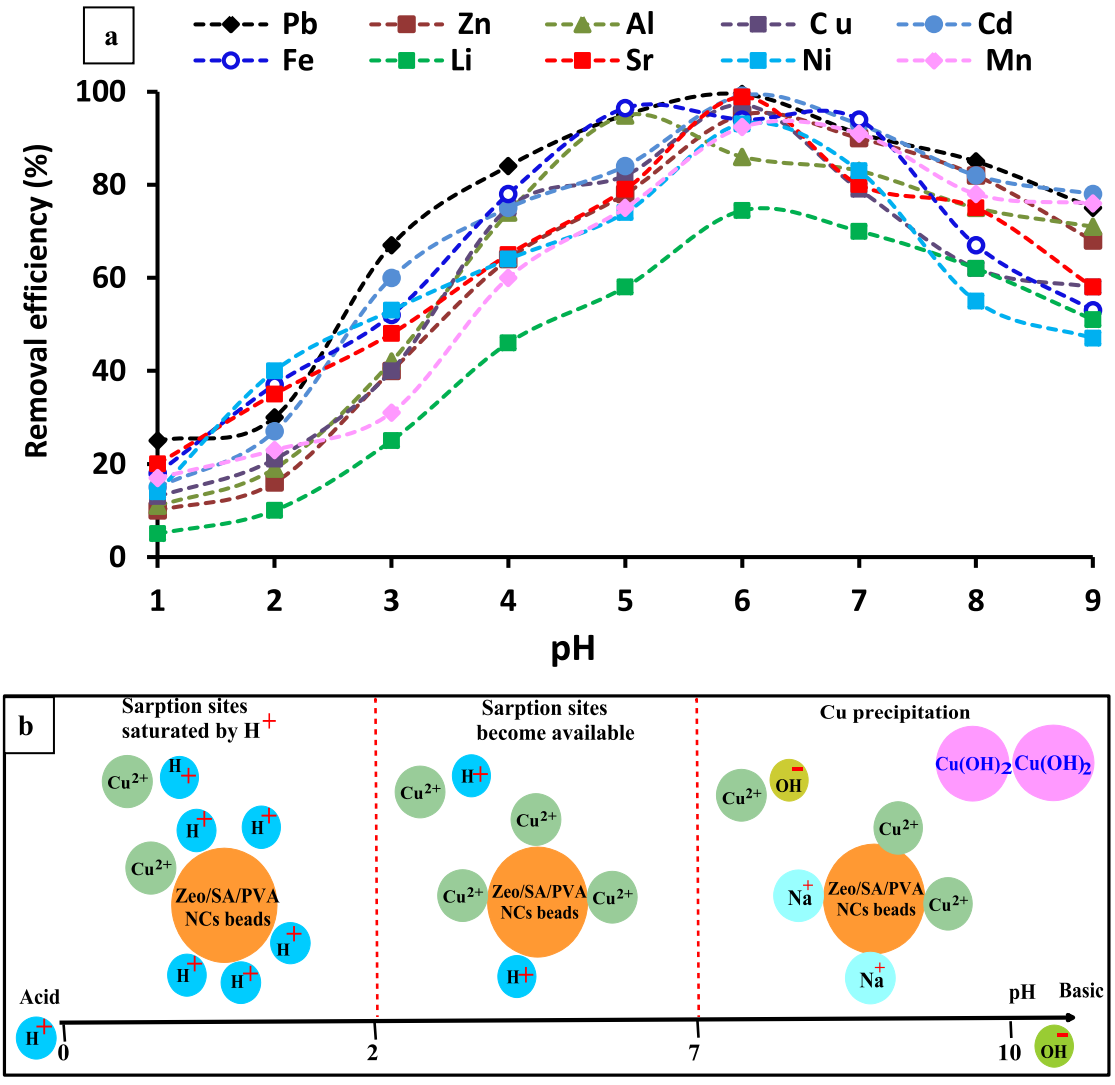

Fig. 10 a) Effect of pH on adsorption of Al^{3+}, Li^{2+}, Fe^{3+}, Ni^{2+}, Sr^{2+}, Cd^{2+}, Cu^{2+}, Zn^{2+}, Mn^{2+} and Pb^{2+}, metal ions concentration 25 mg/L, Temp. = 25 °C, pH = 3–8, contacting time 24 h, adsorbent dose is 20 g/L; b) Effect of pH on the adsorption of heavy metals (ex.: Cu^{2+}) onto Zeo/PVA/SA NCs beads at lower pH, the adsorption sites are saturated by H^+, and the adsorption of Cu^{2+} ions is low, when the pH increases, the sorption sites become available, and the adsorption of Cu^{2+} ions increases. At higher pH, the Cu^{2+} precipitated and Na^+ competes with the residual Cu^{2+}.

be described via the increasing quantity of Na^+ in the solution owing to pH modification which competes with the residual metal ions on the exchangeable spot. This is mainly owing to the decline in the electrostatic interaction among ions and the ionic spots relatively than the competitive adsorption of Na^+ because the Na^+ did not occurred in the removal from the adsorbed beads. It could be expected that the adsorption of metal ions improved with a slight increase in pH, where the metal ionic sorts turn into less stable in the solution because of the surface complexation or via ion exchange with other ions bound to an acidic functional group or by both mechanisms [Yin et al., 2007]. For instance, carboxylic groups (—COOH) are essential groups for metal uptake via organic materials [Ajmal et al., 2000]. The carboxylic groups (—COOH) are deprotonated and turned into negatively charged at a pH higher than 3–5. When the pH getting higher than 3–5, carboxylic groups (—COOH) are deprotonated and negatively charged. Therefore, the attraction of the positively charged ions could be developed [Norton and Baskaran, 2004]. Increasing of pH rate after saturation, does not increase the metal uptake, but fractional metal desorption may take place because of the reaction of metal ions with OH^- ions and precipitate as a metal hydroxide [Farooq et al., 2010]. Furthermore, precipitate could happen at a higher pH value. Therefore, all the experiments were done at the best pH according to the type of each metal ion to obtain the higher removal efficiency in addition to avoid precipitation of metal ions. The maximum adsorption capacity of Zeo/SA/PVA NCs beads for the removal of Al^{3+}, Li^{2+}, Fe^{3+}, Ni^{2+}, Sr^{2+}, Cd^{2+}, Cu^{2+}, Zn^{2+}, Mn^{2+} and Pb^{2+} metal ions is compared with other adsorbents described in previous publications, Table 1. From the table, it is clear that Zeo/SA/PVA NCs beads have the highest maximum adsorption capacity when compared to other adsorbents. This is mainly owing to

Table 1 Comparison of the heavy metal removal efficiency by using different adsorbents.

Adsorbent	Conditions	The maximum removal efficiency (MRF)	Ref.
Poly (vinyl alcohol)/sodium alginate nanofibers.	pH, 5 & Temp, 50 °C & Time, 100 min using 0.002 g PVA/SA nanofiber and 40 ppm Cd^{+2} ions.	67.05 mg/g for Cd ion.	Ebrahimi et al., 2019
(Cr(III)-PVA/SA) membrane.	pH, 6 & Temp, 25 °C & Time, 120 min using 0.5 g/L (Cr(III)-PVA/SA) membrane and 50 mg/L, Cr^{+3} ions.	Maximum adsorptionCapacity (MAC) (mg/g) of Cr^{+3} ions = 59.91 mg/g	Chen et al., 2010
Sodium Alginate/Graphene Oxide Composite Double-Network. Hydrogel Beads (GO/SA).	pH, 6 & Temp, 45 °C & Time, 250 min using 150 mg (GO/SA) beads.	MAC= (mg/g) of Mn^{+2} ions = 56.49 mg/g.	Yang et al., 2018
PVA-Sodium alginate beads (PVA:SA).	Time 1.5 h using 12:2.5 g PVA:SA beads.	99% for Cr (VI)	Chuan et al., 2018
Copper–zeolite X composite.	Time, 45, 45, 60 min for Pd, Cd and Cr using Cu-Z composite.	90.7, 97.7 and 100% for Pb, Cd and Cr respectively.	Fanta et al., 2019
Magnetic zeolite(MZ).	pH, 5.5 & Temp, 25° C & Time, 10 min using 0.7 g /L, and 1 g/L for Cd(II) and Pb(II), respectively.	95 and 89 for Pb and Cd, respectively.	Safinejad et al., 2017
Zeolite/cellulose acetate blend (ZCAB) fiber	pH, 5.5 & Temp, 25° C, Time 48 h, initial metal ion concentration 19 mg/L; bed depth 15 cm; and flow rate 5.4 ml/min.	95.4% for Cu ions.	Ji et al., 2013
Cellulose/sodium alginate (SA) modified with polyethyleneimine (PEI) as an adsorbent (PEI-RCSA).	pH, 5–6& Temp, 25° ± 1 °C & Time, 8 h.	MAC = Cu(II), Zn(II), and Pb(II) were 177.1, 110.2 and 234.2 mg/g, respectively.	Zhan et al., 2018
Magnetic zeolite nanoparticles (MZNCs).	pH, 5–6 & Temp, 27° C & Time, 20 min for Cu (II) and Zn(II) and 30 min for Al(III) using 0.1 g (MZNCs).	98.7, 95.9% and 86.06% for Cu and Zn and Al (III), respectively.	Shalaby et al., 2018
Zeo/SA/PVA NCs beads.	pH, 6.0 for Pb^{2+}, Cd^{2+}, Sr^{2+}, Cu^{2+}, Zn^{2+}, Ni^{2+}, Mn^{2+} and Li^{2+} while pH = 5 for Fe^{3+} and Al^{3+}& Temp, 25° C & Time, 120 min 2 g SA, 1 g PVA and 0.2 g Zeo NPs.	99.5, 99.2, 98.8, 97.2, 95.6, 93.1, 92.4 96.5, 94.9%, and 74.5% for Pb^{2+}, Cd^{2+}, Sr^{2+}, Cu^{2+}, Zn^{2+}, Ni^{2+}, Mn^{2+}, Fe^{3+}, Al^{3+} and Li^{2+}, respectively.	This work

comprising the adsorbent onto multi-functional groups that improving the number of oxygen functional groups (COOH and OH groups) of Zeo/SA/PVA NCs beads that are increased the active sites for heavy metal ions chelation.

5. Adsorption kinetics and isotherms study

5.1. Adsorption kinetics study

The adsorption kinetics tests took place at an adsorbent dose of 20 g/L, metal ions concentration in the range of 5–55 mg/L, at 25 °C. The study of the sorption kinetics offers suitable statistics around the adsorption efficiency and the adsorption mechanisms. For kinetic determination, pseudo-first-order (PFO) and pseudo-second-order (PSO) models were applied to determine the adsorption kinetics. The PFO model refers to the rate of adsorption as to the number of unfilled spots by the solutes and can be expressed via using the simple Lagergren equation [Lagergren 1898]:

$$\mathbf{Log}\ (\mathbf{q_e} - \mathbf{q_t})\ = \log\ \mathbf{q_e} - \mathbf{k_1 t} \tag{4}$$

where q_e and q_t (mg/g) are the quantity of adsorbent phase concentrations at stability and at time t, respectively and k_1 (1/min) is the ratio constant of the pseudo-first-order adsorption [Lagergren 1898]. From scheming log (q_e-q_t) versus t Fig. 11a, the q_e and k_1 were achieved from the intercept and slope, respectively. The PSO model is determined via the equation of Ho and McKay [1999] as follows:

$$\mathbf{t/q_t} = \mathbf{1/k_2 q_e^{\,2}} + \mathbf{t/q_e} \tag{5}$$

where k_2 [g/(mg min)] is the ratio constant of the pseudo-second-order adsorption. From representing t/q_t versus t Fig. 11b, the values of q_e and k_2 were determined from the slope and intercept, respectively. The chemisorptions are typically regarded by way of the rate significant step for adsorption procedures subsequent pseudo-second-order kinetics [Ho and McKay 1999].

The parameters of the two models are demonstrated in Table 2 and Fig. 11a and b. As can be detected from Table 2, the calculated ($q_{e,\ (cal)}$) values match with the experimental ones ($q_{e,\ (exp)}$) that are reflected the applicability of Zeo/PVA/SA NC beads in the treatment of wastewater samples that contain low and high concentrations of the heavy metals. Due to the low correlation coefficient ($R^2 > 0.93$), first-order kinetics model is not enough to describe Al^{3+}, Li^{2+}, Fe^{3+}, Ni^{2+}, Sr^{2+}, Cd^{2+}, Cu^{2+}, Zn^{2+}, $Mn^{2+}$and Pb^{2+} metal ions adsorption onto Zeo/PVA/SA NCs beads. The correlation

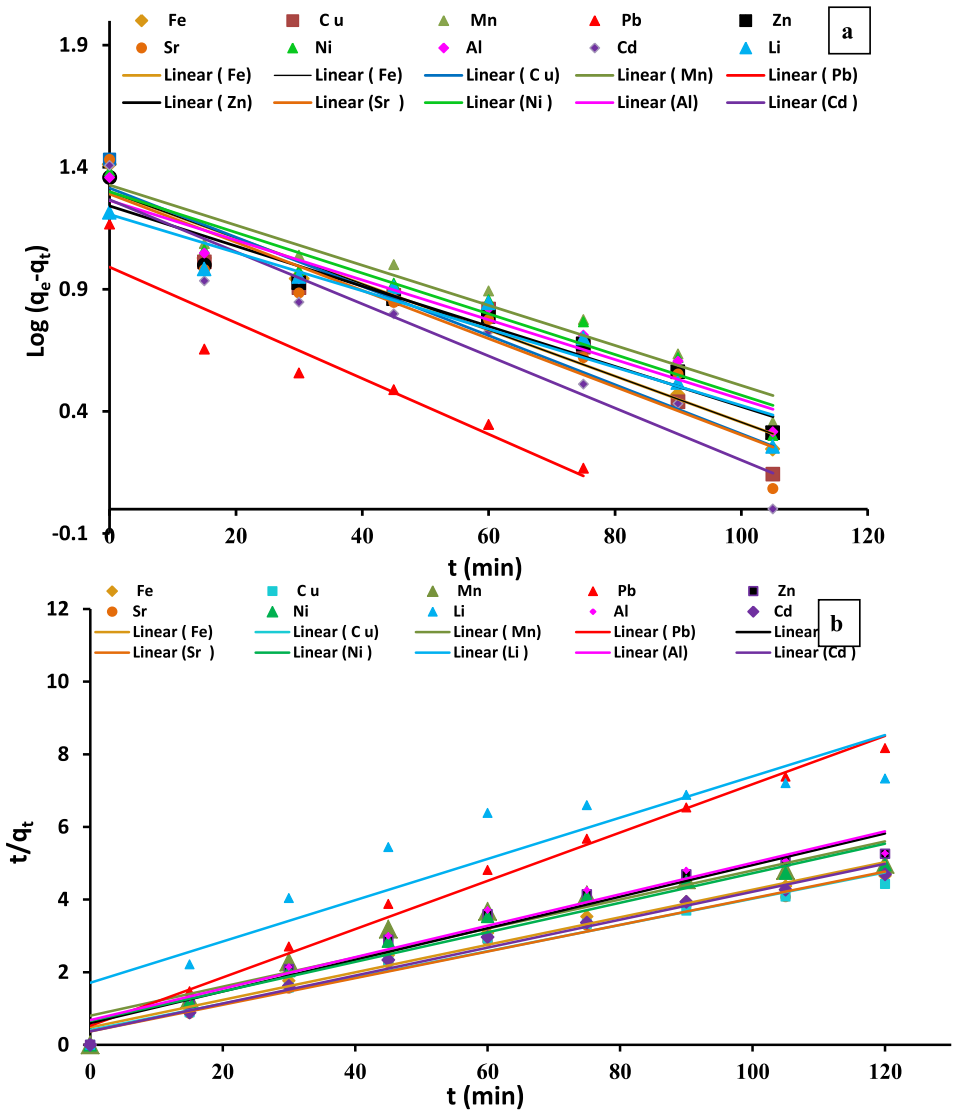

Fig. 11 Kinetic parameters fit of Al^{3+}, Li^{2+}, Fe^{3+}, Ni^{2+}, Sr^{2+}, Cd^{2+}, Cu^{2+}, Zn^{2+}, Mn^{2+} and Pb^{2+} metal ions onto Zeo/PVA/SA NC beads: pseudo-first-order kinetic fit (a), pseudo-second-order kinetic fit (b).

Table 2 Kinetic parameters of Al^{3+}, Li^{2+}, Fe^{3+}, Ni^{2+}, Sr^{2+}, Cd^{2+}, Cu^{2+}, Zn^{2+}, Mn^{2+} and Pb^{2+} metal ions onto Zeo/PVA/SA NC beads.

Metal ions	1st order			Experimental	2nd order		
	$q_{e,calc}$	$K_{1,ad}$ (g/mg. min^{-1})	R^2	$q_{e,exp}$	$q_{e,calc}$	$K_{2,ad}$ ($g.mg^{-}.min^{-1}$)	R^2
Fe	19.95	0.0216	0.946	25.79	26.32	0.0030	0.971
C u	20.66	0.0233	0.919	27.12	27.62	0.0032	0.920
Mn	21.25	0.0189	0.938	24.14	25.00	0.0020	0.989
Pb	3.34	1.2072	0.989	14.69	15.04	0.0084	0.959
Zn	17.44	0.0189	0.935	22.83	22.99	0.0032	0.975
Sr	19.51	0.0228	0.884	27.01	27.25	0.0036	0.944
Ni	19.94	0.0191	0.921	24.20	24.57	0.0025	0.838
Li	16.11	0.0180	0.921	16.37	17.61	0.0019	0.949
Al	18.39	0.0187	0.936	22.78	23.09	0.0027	0.980
Cd	18.52	0.0246	0.908	25.56	26.04	0.0040	0.968

coefficient first-order kinetics model indicates that the pseudo-second-order (PSO) model could be a demonstrative of the reaction mechanism due to it has the higher $R^2 > 0.95$, meanwhile, the calculated value of adsorption saturation ($q_{e\ (cal)}$) from PSO model equation is matched to the actual experimental values of adsorption saturation ($q_{e\ (exp)}$). These outcomes indicating a chemical sorption reaction that occurs in Fig. 11 b which is matches with the thermodynamic studies. The PVA and SA offer sufficiently of COOH and OH reactive sites, and Zeo NPs offer surface OH functional groups, which can be consumed as active adsorption spots with the selected metal ions. The adsorption rate improved with the increase of contacting time of the particular metal ions which confirmed via the PSO model. This phenomenon is indicated to the presence of abundant adsorption site of Zeo/PVA/SA NCs beads are available at a certain time, the adsorption quantity reached the equilibrium, which reveals that most of the active sorption spots on the synthesized beads have been dominated via particular metal ions.

5.2. Adsorption isotherms

To realize the spreading of the metal ions on the adsorption procedure and the adsorbent surface, it is essential to apply the adsorption isotherms. Adsorption equilibrium models of Langmuir and Freundlich were considered to determine the correlation of metals adsorption with various induced concentrations. The greatest suitable isotherm was estimated via linear relapse, and the factors got from the intercept and slope of the linear plots of these models. The widespread usage of the Langmuir isotherm model is described via the following equation:

$$\mathbf{C_e/q_e = 1/(q_m k_L)\ + C_e/q_m} \tag{6}$$

where q_e and q_m are the adsorption quantity at stability (mg/g) and the adsorption capacity (mg/g), respectively, k_L (L/mg) is the Langmuir sorption constant, and C_e (mg/L) is the stability element ion concentration in solution. The values of k_L and q_m can be achieved from the intercept and slope of the relation between C_e/q_e as opposed to C_e, Table 3 and Fig. 12a.

Freundlich isotherm model is expressed through the subsequent equation:

$$\mathbf{Log\ q_e = \log K_f + (1/n)\ \log\ C_e} \tag{7}$$

where C_e (mg/L) is the stability metal ion concentration in aqueous solution, q_e (mg/g) is the stability metal ion concentration on the adsorbent, K_f (l/mg) and n are the Freundlich constants which can be associated to the adsorption capacity of the Zeo/PVA/SA NCs beads and the adsorption intensity, respectively, as well as (1/n) show the heterogeneity of the surface of the bead [Quinones and Guiochon 1996]. The values of K_F and 1/n can be achieved from the intercept and slope of against the relation between log q_e versus log C_e, Table 3 and Fig. 12b.

As can be detected from Table 3 and Fig. 12a and b, the experimental ($q_{e(exp)}$) values contest with the calculated ($q_{e\ (cal)}$) value that is considered in the level of high concentrations. These outcomes reveal the applicability of adsorption in the purification of wastewater samples that have lower and higher concentrations of metal ions. Conversely, K_L values show the adsorption affinity of the binding spots where the good adsorption is shown via lower values of Langmuir factor [Kumar et al. 2005]. This statement is confirmed as the higher (K_L) calculated values are found to be inversely proportional to the actual high adsorption capacities (qe $_{(exp)}$) and vice versa. The values of Freundlich factor (n) that are greater than unity show the favorability of the Zeo/PVA/SA NCs beads to adsorb heavy metals from wastewater. Also, the greater adsorption capacity (K_F) shows the strong electrostatic attraction force [Kumar et al., 2005]; consequently, the higher (K_F) calculated values are found to be proportional to the actual high adsorption capacities (qe $_{(exp)}$) and vice versa.

The best-fit equilibrium model was detected according to the linear regression correlation coefficient (R^2) which showed in Table 3 and Fig. 12a and b. The results displayed that the adsorption procedure fitted well with the Langmuir isotherm model than the Freundlich isotherm model for Al^{3+}, Li^{2+}, Fe^{3+}, Ni^{2+}, Sr^{2+}, Cd^{2+}, Cu^{2+}, Zn^{2+}, Mn^{2+}, and Pb^{2+} metal ions. The outcomes specified that the Langmuir sorption isotherm model represented the adsorption procedure more

Table 3 Results gotten from Langmuir and Freundlich adsorption isotherm models for for Al^{3+}, Li^{2+}, Fe^{3+}, Ni^{2+}, Sr^{2+}, Cd^{2+}, Cu^{2+}, Zn^{2+}, $Mn^{2+}$and Pb^{2+} metal ions onto Zeo/PVA/SA NC beads.

Metal ions	Langmuir model			Experimental	Freundlich model		
	$q_{m,calc}$ (mg/g)	K_L	R^2	$q_{e,exp}$	n	K_f (mg/g)	R^2
Fe	47.170	1.140	0.995	44.52	2.304	19.53	0.950
C u	48.544	1.401	0.989	47.15	2.554	22.31	0.934
Mn	46.296	0.421	0.990	40.82	1.987	12.31	0.922
Pb	47.619	4.375	0.981	48.59	1.659	31.49	0.874
Zn	48.309	0.770	0.991	44.74	2.146	17.44	0.924
Sr	47.170	2.524	0.987	47.11	2.956	26.19	0.900
Ni	47.619	0.469	0.991	41.75	1.926	13.18	0.933
Li	38.314	0.126	0.996	29.55	1.659	4.85	0.960
Al	49.261	0.606	0.992	43.68	1.876	15.25	0.913
Cd	46.296	3.429	0.985	46.63	3.333	28.58	0.923

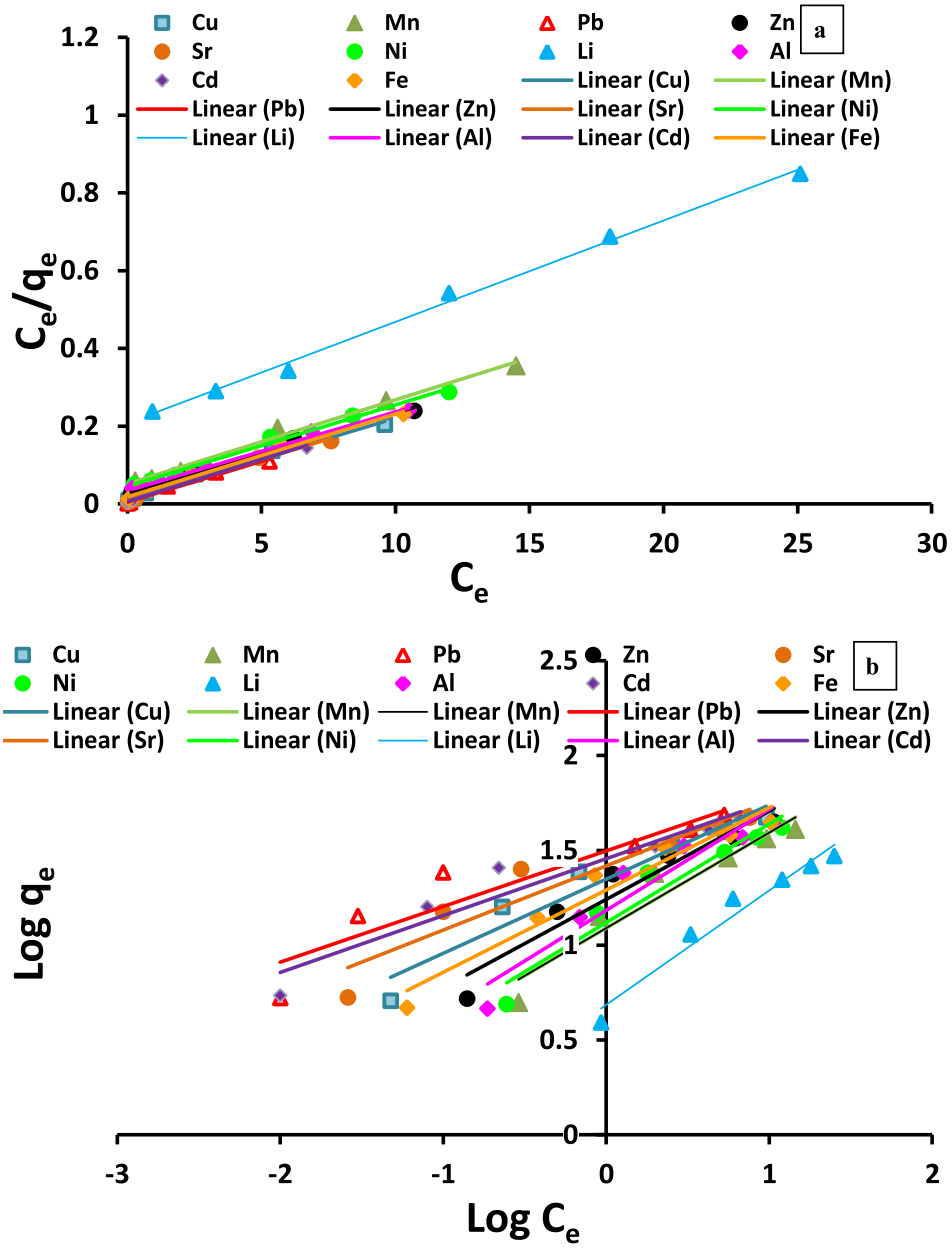

Fig. 12 Linearized Langmuir (a) and Freundlich (b) adsorption isotherm models for Al^{3+}, Li^{2+}, Fe^{3+}, Ni^{2+}, Sr^{2+}, Cd^{2+}, Cu^{2+}, Zn^{2+}, Mn^{2+} and Pb^{2+} metal ions onto Zeo/PVA/SA NC beads.

ideally, which mainly due to the homogeneous nature of the selected metal ions adsorption onto Zeo/PVA/SA NCs beads and suggested the adsorption of metal ions onto the synthesized beads are monolayer coverage. The adsorption mechanism could be mostly owing to the creation of a single layer of ions on the Zeo/PVA/SA NCs bead surface and the active spots of the constituents. As the SA beads modified using PVA and Zeo NPs so more reactive groups as OH and COOH are available to interact with the metal ions of the aqueous solution, as well as more active spots are obtainable, which could be occupied by metal ions, are existing in the constituents.

5.3. Thermodynamic studies

The impact of temperature on the adsorption procedure can be described via computing the thermodynamic parameters as alterations in standard free energy (ΔG), entropy (ΔS) and enthalpy (ΔH) which can be calculated via using the following equations:

$$\mathbf{K}_c = C_a/C_e \tag{8}$$

$$In\, K_c = (-\Delta H/R)\cdot(1/T) + (\Delta S/R) \tag{9}$$

$$\Delta G = \Delta H - T\Delta S \tag{10}$$

where K_c is the distribution ratio among adsorbent into an aqueous solution and metal ions, C_a is the adsorbed element (initial-final concentrations) (mg/L), C_e is the residual (final concentration) (mg/L), T is the temperature (K), R is the gas constant (8.314 J/ mol K), ΔH is the alteration in enthalpy (heat content) (J/mol), ΔS is the alteration in entropy (randomness) (J/ mol K), and ΔG is the alteration in Gibbs' free energy of element removal (J/mol). The ΔS and ΔH values can be gotten from the intercept and slope, respectively, of the Van't Hoff relationship of ln K_c against 1/T. Furthermore, ΔG values are considered based on ΔS and ΔH values.

The Van't Hoff relationship among ln K_c against 1/T for the synthesized Zeo/PVA/SA NC beads is displayed in Table 4 and Fig. 13. Following the revealed equations, the slopes and intercepts of straight lines in Fig. 13, thermodynamic factors were calculated, and are offered in Table 4.

The data gotten from the adsorption tests at various temperatures are utilized to evaluate the thermodynamics parameter for Al^{3+}, Li^{2+}, Fe^{3+}, Ni^{2+}, Sr^{2+}, Cd^{2+}, Cu^{2+}, Zn^{2+}, $Mn^{2+}$and Pb^{2+} metal ions onto Zeo/PVA/SA NC beads. The present outcomes in Table 2 and Fig. 13 showed that Van't Hoff's pattern of ln Kc against 1/T is considered fitting owing to the great number of correlation values (R^2). The positive values of (ΔH) display the endothermic procedure, which is an indication of the presence of a resistant interaction among Zeo/SA/PVA NCs beads and the selective metal ions. Moreover, the positive amounts of (ΔH) are responsible for the decrease in adsorption ratio via increasing in temperature. The higher positive values of ΔH propose the possibility of strong bonding among the adsorbent and adsorbate. The positive enthalpy (ΔH) of adsorption achieved identifies the chemical adsorption process. This proposes that the chemical bonds

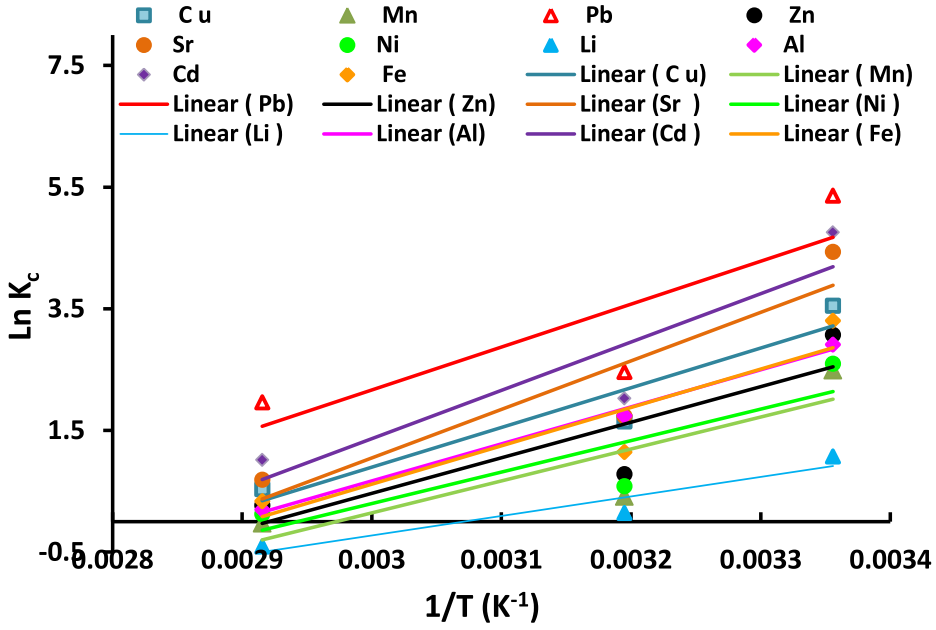

Fig. 13 Van't Hoff Plot of ln K_c versus 1/T for Al^{3+}, Li^{2+}, Fe^{3+}, Ni^{2+}, Sr^{2+}, Cd^{2+}, Cu^{2+}, Zn^{2+}, $Mn^{2+}$and Pb^{2+} metal ions onto Zeo/PVA/SA NC beads.

Table 4 Thermodynamic parameters for Al^{3+}, Li^{2+}, Fe^{3+}, Ni^{2+}, Sr^{2+}, Cd^{2+}, Cu^{2+}, Zn^{2+}, $Mn^{2+}$and Pb^{2+} metal ions onto Zeo/PVA/SA NC beads.

Metal ions	Thermodynamic parameters							
	Δ H (j/mol)	ΔS (j/mol.K)			ΔG (j/mol)			R^2
		298	313	343	298	313	343	
Fe	52,416	176	167	153	−8181	−9237	−7100	0.8397
C u	54,305	298	313	343	−34499	−43664	−63344	0.9108
Mn	43,708	176	167	153	−8707	−8707	−8707	0.8589
Pb	58,705	298	313	343	−30099	−39264	−58944	0.86
Zn	48,709	176	167	153	−3706	−3706	−3706	0.8659
Sr	66,320	298	313	343	−22484	−31649	−51329	0.9452
Ni	43,078	176	167	153	−9337	−9337	−9337	0.969
Li	26,693	298	313	343	−62111	−71276	−90956	0.9125
Al	50,687	176	167	153	−1728	−1728	−1728	0.9943
Cd	66,136	298	313	343	−22668	−31833	−51513	0.8389

among the Zeo/SA/PVA NCs beads surfaces and the heavy metal molecules are strong enough and the heavy metal molecules cannot be desorbed on the Zeo/SA/PVA NCs beads via physical properties such as heating or simple shaking [Farah and El-Gendy 2013]. The positive values of (ΔS) indicate the increased randomness at the solid/solution interface throughout the adsorption of the selected metal ions on Zeo/PVA/SA NC beads, indicating that the metal particles were systematically adsorbed on the surface of the Zeo/SA/PVA NCs beads. This indicates less imperative in the reaction among the adsorbent and adsorbate (less order in the structure among the adsorbent and adsorbate). The negative values of (ΔG) specified the spontaneous nature of adsorption for the tested metals using Zeo/PVA/SA NC beads which representing an improvement in the achievability of adsorption at lower temperatures. Summarizing these results, the adsorption mechanism of the selective studied metal ions is endothermic, chemical, spontaneous adsorption on the surface of the Zeo/PVA/SA NC beads.

6. Recovery and reusability of adsorbents

Reusability of the metal adsorbents can diminish the cost of heavy metal elimination in repetition. In the field of wastewater purification technologies, the challenge is to find constituents with high adsorption capability without damaging that may be easily removed from the polluted media. Regeneration of the chelating beads after metal sorption procedure devoid of damaging the capacity is a very essential issue for the success of sorption technology improvement. From the economic fact of outlook, it is estimated that such ingredients could be used for several cycles without dropping their adsorption capacity, or at least with slight loss. In this work, the adsorption propensity was verified as a long ten successive adsorption–desorption series.

Reusability of various metal ions adsorbed on Zeo/PVA/SA NCs beads was carried out using 0.1 M HCl as an adsorbing agent with continuous shaking at 180 rpm for 1 h at 25 °C. The values achieved using Zeo/PVA/SA NCs beads after ten adsorption–desorption series are shown in Fig. 14. The regeneration stability was confirmed by applying the adsorption and desorption procedures numerous times. The experiment displays that a significant decrease in the sorption capacity after 10 repeating cycles. The sorption capacity decreases from 99.5, 99.2, 98.8, 97.2, 96.5, 94.9, 95.6, 93.1, 92.4 and 74.5% for Pb^{2+}, Cd^{2+}, Sr^{2+}, Cu^{2+}, Fe^{3+}, Al^{3+}, Zn^{2+}, Ni^{2+}, Mn^{2+} and Li^{2+} ,respectively to 92, 91, 90, 89, 87, 85, 86, 83, 85 and 86% for Pb^{2+}, Cd^{2+}, Sr^{2+}, Cu^{2+}, Fe^{3+}, Al^{3+}, Zn^{2+}, Ni^{2+}, Mn^{2+}, and Li^{2+} ions of their initial adsorption ability, respectively. The result showed that the synthesized Zeo/PVA/SA NCs beads could be successfully used for treating wastewater having Pb^{2+}, Cd^{2+}, Sr^{2+}, Cu^{2+}, Fe^{3+}, Al^{3+}, Zn^{2+}, Ni^{2+}, Mn^{2+}, and Li ions at least for ten times.

7. Antibacterial properties of the synthesized beads

The improvement of effective and low-cost technology is required to address the problems related to the harmful influences of microorganisms on the synthesized beads. The antibacterial removal is one of the highest challenges in separation procedures, where immersed beads, in pure or wastewater, appeal microorganisms containing diatoms, bacteria, and algae. The microorganisms in water and wastewaters create a severe ecological problem, producing concern worldwide. Therefore, various alternatives were deliberated to contribute an effective and economical solution. The inexpensive and the abundance of natural Zeo NPs along with their greater features and high exchange capabilities agreeable its usage as a low-cost adsorbent ant a carrier of immobilized microorganisms or biofilm [Foglar and Kljic 2011]. In this study, the effective elimination of Escherichia coli (E. coli) from aqueous solutions was described using SA, PVA/SA and Zeo/PVA/SA NCs beads. The bactericidal ability of SA, PVA/SA and Zeo/PVA/SA NCs beads was confirmed via measuring E. coli (initial concentration = 10^{+8} CFU/ml) survival. Fig. 15 displays the E. coli removal efficiency in the water on different SA, PVA/SA and Zeo/PVA/SA NCs beads. The antibacterial properties of the SA and PVA/SA beads were considerably enhanced via the addition of Zeo NPs. The survival count (%) of the E. coli cells was 34% on the SA beads,

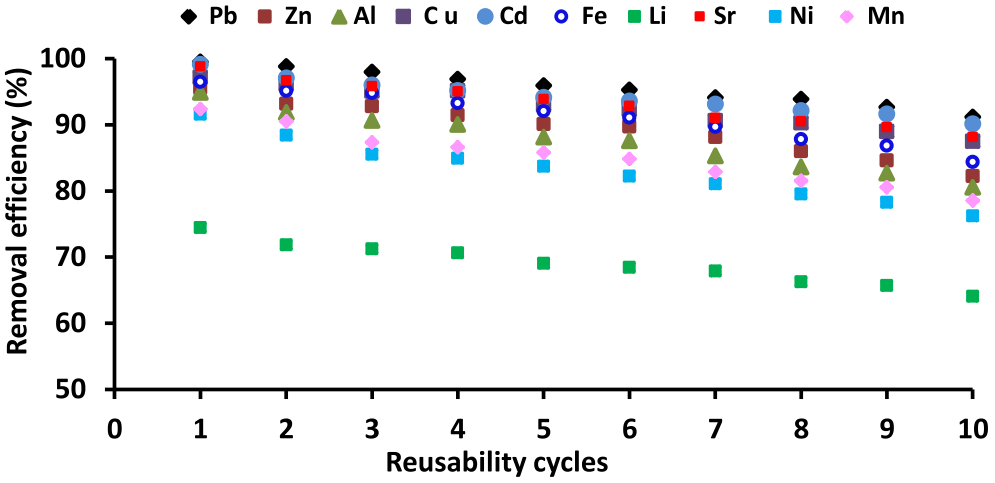

Fig. 14 Effect of reusability on the efficiency of Zeo/PVA/SA NCs beads towards the selective metal ions, Metal ions concentration 25 mg/L, Temp. = 25 °C, at ambient pH according to the type of metal ions, adsorbent dose is 20 g/L.

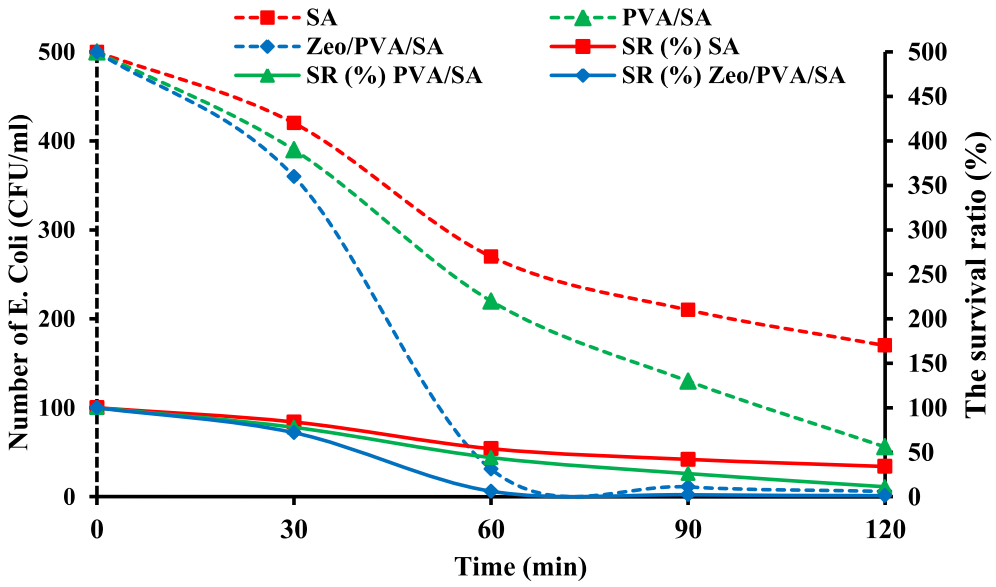

Fig. 15 The cell number and survival ratio curve of E. coli in SA, PVA/SA and Zeo/PVA/SA NC modified beads.

11% on the PVA/SA, and 1% on the Zeo/PVA/SA NC modified beads, after 120 min exposure at 25 °C. These outcomes were related to the initial concentrations of the E. coli solution. E. coli survival was highest on the SA beads and lowest on the Zeo/PVA/SA NCs beads at 25 °C. In comparison, the SA beads alone exhibited slightly less antibacterial activity [Kumar et al., 2019], where the antibacterial activity of the SA was significantly improved by the incorporation of PVA to the polymer matrix [Rafiq et al., 2018]. This mainly due to reactive functional groups into Zeo/PVA/SA NCs beads as OH, COOH groups can improve the negative surface charge of the Zeo/PVA/SA NCs beads which increases the antibacterial abilities of the synthesized beads, because of the negative surface charge of E. coli [Rezaee et al., 2011]. These outcomes show, that the Zeo NPs modified the Zeo/PVA/SA NCs beads can remove E. coli further efficiently than neat SA and PVA/SA beads, because of the antibacterial effect of the Zeo NPs. Almost complete elimination of E. coli occurred within 120 min exposure on Zeo/PVA/SA NCs beads. The bactericidal effect of Zeo NPs is due to its catalytic activity [Jahangirian et al., 2013] and antifouling possessions that oxidize structures and destroy the outer-shell of bacteria cells. Moreover, these outcomes also match with those reported by [Zendehde et al., 2016], as concerns their belongings on various microbial groups are disturbed. These outcomes are constant with the findings that Zeo NPs have superior efficiency in degradation reactions, and offer ecological and economic benefits compared to conventional approaches.

8. Application for removal efficiency

Groundwater has generally been presumed to be safe for utilization without purification. In Egypt, many areas rely on groundwater as the individual water resource for various uses. Throughout the last decayed, heavy metals investments have been dedicated to turning territories of the infertile desert into green creative areas, to continue the highly increasing ratio of population. The purification of wastewater from domestic agricultural or industrial activities to groundwater depends on the capacity and activities of the pollutants as well as hydrogeological and geological aspects that device the flow and distribution of the pollutants. The 10th of Ramadan city is one of the new dominions that are created the boundaries near or close to Cairo city to outspread the occupational region and to discharge the socio-economic strains assuming Cairo because of overpopulation and improvement observes. The 10th of Ramadan city include large industrial companies over 1130 dispersed in three areas and contains various activities such as the manufacture of detergent textile production, electroplating, petroleum manufacturing, iron, and steel factory, battery fabrications, etc. The providing production wells (withdrawal is about 25000 m^3 /day) are mixed with treated surface water in the pipeline and utilized for drinking, domestic and manufacturing purposes. The wastewater discharge reaches about 280,000 m^3/day, the human activity 20% and the manufacturing drainage exemplified 80%. All wastewater is discharged into three oxidation ponds for contaminant's decline and expenditure of charges.

The chemistry of four groundwater samples was estimated via the analysis of major cations and anions in addition to the minor elements as heavy inorganic elements Tables 5 and 6. The chemical analyses were estimated in the Central laboratory of the Desert Research Center. The outcomes displayed that the chemical inorganic concentration of Al^{3+}, Fe^{3+}, Cr^{3+}, Co^{2+}, Cd^{2+}, Zn^{2+}, Mn^{2+}, Ni^{2+}, Cu^{2+}, Li^{2+}, Sr^{2+}, Si^{2+}, V^{2+}, and Pb^{2+} in all wastewater samples are greater than the acceptable limits according to WHO 2006 and the Egyptian Standards 2007 see Table 6**.** Furthermore, most samples of wastewater oxidation ponds were contaminated with Al^{3+}, Fe^{3+}, Cr^{3+}, Co^{2+}, Cd^{2+}, Zn^{2+}, Mn^{2+}, Ni^{2+}, Cu^{2+}, Li^{2+}, Sr^{2+}, Si^{2+}, V^{2+}, and Pb^{2+} ions, and this reflects domestic activities and manufacturing in the study region. Due to the higher concentrations of these metal ions, so, an experiment has been prepared in this work to treat this groundwater utilizing the synthesized Zeo/PVA/SA NC beads. Four groundwa-

Table 5 Chemical (meq/l) data for the collected samples.

Sample No.		pH	EC ms/cm	TDS mg/l	Unit	Ca	Mg	Na	K	Total Cation	CO_3	HCO_3	SO_4	Cl	Total Anion
1	Before	3.8	5560	3062	ppm	297	94	620	57	51.0	0	0	966	1028	49.1
					epm	14.8	7.7	27.0	1.5		0	0.0	20.1	29.0	
	After	3.1	5480	2045	ppm	184	85	420	54	35.8	0	0	300	1003	34.5
					epm	9.2	7.0	18.3	1.4		0	0.0	6.2	28.3	
2	Before	7.6	10,420	6274	ppm	297	126	1500	62	92.0	0	122	1143	3085	112.8
					epm	14.8	10.4	65.2	1.6		0	2.0	23.8	87.0	
	After	5.3	9250	5040	ppm	180	125	1450	56	83.7	0	122	700	2468	86.2
					epm	9.0	10.3	63.0	1.4		0	2.0	14.6	69.6	
3	Before	7.4	10,090	5590	ppm	287	115	1600	56	94.8	0	142	315	3147	97.6
					epm	14.3	9.5	69.6	1.4		0	2.3	6.6	88.7	
	After	7.1	8940	4877	ppm	257	112	1550	51	90.8	0	138	289	2549	80.1
					epm	12.8	9.2	67.4	1.3		0	2.3	6.0	71.9	
4	Before	7.6	6970	3698	ppm	260	100	900	40	61.4	0	0	520	1878	63.8
					epm	13.0	8.2	39.1	1.0		0	0.0	10.8	53.0	
	After	7.2	6820	3129	ppm	254	90	802	35	55.9	0	0	254	1694	53.1
					epm	12.7	7.4	34.9	0.9		0	0.0	5.3	47.8	
WHO		6.5-9.2	.....	1000		.....	.....	200	.....	.....	.....	.....	500	250	.....
E. S 2007		6.5-8.5	.....	1000		350	150	200	.....	.....	.....	.....	250	250	.....

Table 6 Heavy metal concentration of the collected samples in the study area.

Sample No.		Al	Cd	Co	Cr	Cu	Fe	Li	Mn	Ni	Pb	Si	Sr	V	Zn
1	**After**	1.241	0.037	0.001	0.020	0.266	2.548	0.045	0.359	0 0.0739	0 0.1597	9.571	4.952	0.021	0.277
	Before	0.2692	0.001	0.000	0.003	0.0390	0.071	0.003	0.015	0.016	0.001	2.062	1.176	0.001	0.0355
	%	**78.3**	**98.4**	**60.0**	**84.5**	**85.3**	**97.2**	**93.2**	**95.9**	**78.4**	**99.4**	**78.5**	**76.3**	**95.2**	**87.2**
2	**After**	1.103	0.071	0.001	0.175	0.194	2.859	0.124	0.273	0.132	0.190	9.514	7.960	0.042	2.960
	Before	0.153	0.018	0.000	0.010	0.019	0.134	0.025	0 0.0233	0.002	0.003	1.943	1.518	0.010	0.037
	%	**86.2**	**74.3**	**60.0**	**94.3**	**90.2**	**95.3**	**79.6**	**91.5**	**98.5**	**98.6**	**79.6**	**80.9**	**76.4**	**98.8**
3	**After**	1.046	0.011	0.075	0.004	0.031	0.322	0.146	0.325	0.075	0.405	14.530	7.121	0.004	0.586
	Before	0.002	0.000	0.000	0.001	0.005	0.019	0.001	0.004	0.015	0.007	3.670	1.135	0.001	0.030
	%	**99.8**	**97.3**	**99.5**	**73.2**	**84.6**	**94.3**	**99.2**	**98.7**	**80.6**	**98.3**	**74.7**	**84.1**	**81.1**	**94.9**
4	**After**	0.299	0.014	0.078	0.014	0.229	0.524	0.130	0.329	0.060	0.215	9.766	5.592	0.014	0.451
	Before	0.012	0.002	0.017	0.003	0.009	0.126	0.005	0.014	0.012	0.057	2.157	0.958	0.004	0.038
	%	**96.2**	**82.6**	**78.4**	**77.4**	**96.0**	**75.9**	**96.5**	**95.9**	**80.9**	**73.3**	**77.9**	**82.9**	**69.9**	**91.6**
Permissible limit (WHO)		**0.2**	**0.003**	**< 0.05**	**0.01**	**< 0.05**	**0.3**	**0.003**	**0.2**	**0.01**	**0.05**	.....	**0.11**	**0.01-0.1**	**5**
Permissible limit (E. S.)		**0.2**	**0.005**	**< 0.05**	**0.05**	**< 0.05**	**0.3**	**0.003**	**0.05**	.....	**0.05**	.....	.....	**0.2**	**3**

Note: The concentration expressed as ppm; permissible limit according to World Health Organization guidelines (WHO 2006, ppm) and Egyptian maximum Permissible limit (Egyptian Standards 2007, ppm).

ter samples collected from various locations in the study location were selected for the treatment procedure. The efficiency of the treatment was estimated via a complete chemical analysis of such groundwater samples before and after the treatment procedure. Tables 5 and 6 display the outcomes of these selected samples. The results of the analysis before the treatment procedure demonstrated that; the salinity of these selected water samples, as well as the concentrations of major

cations and anions (Ca^{2+}, Mg^{2+}, Na^{+}, K^{+}, HCO_3^-, SO_4^{2-}, and Cl^-), are all greater than the suitable limits for drinking according to WHO standard. Alternatively, higher concentrations of Al^{3+}, Fe^{3+}, Cr^{3+}, Co^{2+}, Cd^{2+}, Zn^{2+}, Mn^{2+}, Ni^{2+}, Cu^{2+}, Li^{2+}, Sr^{2+}, Si^{2+}, V^{2+} and Pb^{2+} are gotten in these samples. Nonetheless, after the treatment procedure, it is realized that the synthesized Zeo/PVA/SA NC beads were able to eliminate 60–99.8% of Al^{3+}, Fe^{3+}, Cr^{3+}, Co^{2+}, Cd^{2+}, Zn^{2+}, Mn^{2+}, Ni^{2+}, Cu^{2+}, Li^{2+}, Sr^{2+}, Si^{2+}, V^{2+}, and Pb^{2+} ions. The analysis also revealed a decline in the (Ca^{2+}, Mg^{2+}, Na^{+}, and SO_4^{2-}), assigning the attraction of the chelated beads towards alkaline earth metals as that for transition metal ions as well as sulfate ions. The reduction in the concentrations of heavy element ions, calcium, magnesium, sodium and sulfate is followed by a large decline in the salinity of the water samples which ranged from 13 to 33%. It can be consequently recommended that the synthesized Zeo/PVA/SA NC beads could be utilized for treatment and desalination procedures.

9. Conclusions

In this work, the author suggests the use of a novel technique to remove heavy metals from wastewater. Efficient Zeo/PVA/SA NC beads have been synthesized via a low cost, easy, and simple technique. The optimum preparation circumstances were 2 g SA, 1 g PVA, and 0.2 g Zeo NPs using water as a solvent and the glutaraldehyde (GA) as cross-linked for beads former procedure. The achieved results revealed that the removal efficiency using Zeo/PVA/SA NC modified beads reached the maximum at the pH value of 6.0 for Pb^{2+}, Cd^{2+}, Sr^{2+}, Cu^{2+}, Zn^{2+}, Ni^{2+}, Mn^{2+} and Li^{2+} with 99.5, 99.2, 98.8, 97.2, 95.6, 93.1, 92.4 and 74.5%, respectively, while the highest removal is achieved at pH = 5 for Fe^{3+} and Al^{3+} with 96.5 and 94.9%, respectively at 25 °C and the equilibrium time of 120 min and the optimal adsorbent dose was 20 g/L. The thermodynamic studies demonstrated that the adsorption mechanisms of the selective metal ions were chemical in nature, endothermic, spontaneous adsorption on the surface of the Zeo/PVA/SA NC beads and the adsorption isotherm was well fitted via the Langmuir isotherm model. Furthermore, the antibacterial activity of Zeo/PVA/SA NC beads was demonstrated by E. coli as a potential source of bacteria's where the survival count (%) of the E. coli cells were 34% on the SA beads, 11% on the PVA/SA, and 1% on the Zeo/PVA/SA NC modified beads, after 120 min exposure at 25 °C. The applicability of Zeo/PVA/SA NC beads for the treatment of natural groundwater samples collected from 10th Ramadan City, Cairo, Egypt was able to eliminate 60–99.8% of Pb^{2+}, Cd^{2+}, Sr^{2+}, Cu^{2+}, Fe^{3+}, Al^{3+}, Zn^{2+}, Ni^{2+}, Mn^{2+}, and Li^{2+} ions, respectively. Reusability experimental shows that the Zeo/PVA/SA NC modified beads preserved a significant decrease in the sorption capacity after 10 repeating cycles. The achieved results demonstrate that the synthesized Zeo/PVA/SA NCs beads were been suggested to be safe, simple and environmentally friendly for purification of the wastewater, improving the selectivity, the antibacterial properties and inexpensive technology for declining the biological quantity in wastewater management procedures and attain a favorable potential in enhancing the quality of water resources.

Acknowledgements

The author would like to acknowledge Dr. Mona El Shazly for the great assistance in Antibacterial properties, tests in Microbiology Department, Desert research center, Egypt.

References

Abdel Salam, O.E., Reiad, N.A., ElShafei, M.M., 2011. A Study of the Removal Characteristics of Heavy Metals from Wastewater by Low-cost Adsorbents. J. Adv. Res. 2, 297–303.

Agrawal, P., Patil, R., Kalyaneb, N., Joshi, U.V.A., 2010. Formulation and in-vitro evaluation of Zidovudine loaded calcium alginate microparticles containing copolymer. J. Pharm. Res. 3, 486–490.

Aguado, J., Arsuaga, J.M., Arencibia, A., Lindo, M., Gascon, V., 2009. Aqueous heavy metals removal by adsorption on ´ amine-functionalized mesoporous silica. J. Hazard. Mater. 163 (1), 213–221.

Ajmal, M., Rao, R.A.K., Ahmad, R., Ahmad, J., 2000. Adsorption studies on Citrus reticulata (fruit peel of orange): removal and recovery of Ni(II) from electroplating wastewater. J. Hazard. Mater. 79 (1), 117–131.

Alfaro-Cuevas-Villanueva, R., Hidalgo-Vazquez, A.R., Cortes Penagos, C.D.J., Cortes-Martinez, R., 2014. Thermodynamic, kinetic, and equilibrium parameters for the removal of lead and cadmium from aqueous solutions with calcium alginate beads. Sci. World J., 1–9

American Public Health Association (APHA), (1995), American Water Works Association, Water Pollution Control Federation, Standard methods for the examination of water and wastewater. Washington: American Public Health Association

Baker, H., Khalili, F., 2007. Effects of pH and temperature on the interaction of Pb (II) with Azraq humic acid by Schubert's ion exchange method. Ann. Environ. Sci. 1, 35–44.

Barala, S.S., Das, N., Chaudhury, G.R., Das, S.N., 2009. A preliminary study on the adsorptive removal of Cr(VI) using seaweed, Hydrilla verticillata. J. Hazard. Mater. 171, 358–369.

Bée, A., Talbot, D., Abramson, S., Dupuis, V., 2011. Magnetic alginate beads for Pb(II) ions removal from wastewater. J. Colloid Interface Sci. 362 (2), 486–492.

Castaldi, P., Santona, L., Enzo, S., Melis, P., 2008. Sorption processes and XRD analysis of a natural zeolite exchanged with Pb^{2+}, Cd^{2+} and Zn^{2+} cations. J. Hazard. Mater. 156, 428–434.

Chen, J.H., Li, G.P., Liu, Q.L., Ni, J.C., Wu, W.B., Lin, J.M., 2010. Cr(III) ionic imprinted polyvinyl alcohol/sodium alginate (PVA/SA) porous composite membranes for selective adsorption of Cr (III) ions. Chem. Eng. J. 165 (2), 465–473.

Chintalapudi, P., Pujar, P., Khadse, G., Sanam, R., Labhasetwar, P., 2017. Groundwater quality assessment in emerging industrial cluster of alluvial aquifer near Jaipur India. Environ. Earth Sci. 76, 8.

Choi, J.W., Yang, K.S., Kim, D.J., Lee, C.E., 2009. Adsorption of zinc and toluene by alginate complex impregnated with zeolite and activated carbon. Curr. Appl. Phys. 9, 694–697.

Chuan, L.T., Manap, N., Abdullah, H.Z., Idris, M.I., 2018. Polyvinyl Alcohol-Alginate Adsorbent Beads for Chromium (VI) Removal. Int. J. Eng. Technol. 7 (3.20), 95–99.

De Queiroz, A.A.A., Passes, E.D., De Brito Alves, S., Silva, G.S., Higa, O.Z., Vítolo, M., 2006. Alginate- poly(vinyl alcohol) Core-shell Microspheres for Lipase Immobilization. J. Appl. Polym. Sci. 102, 1553–1560.

Dragan, E.S., Apopei Loghin, D.F., Cocarta, A.I., 2014. Efficient sorption of Cu2+ by Composite Chelating Sorbents Based on Potato Starch- Graft -Polyamidoxime Embedded in Chitosan Beads. ACS Appl. Mater. Interfaces. 6, 16577–16592.

Ebrahimi, F., Sadeghizadeh, A., Neysan, F., Heydari, M., 2019. Fabrication of nanofibers using sodium alginate and Poly(Vinyl alcohol) for the removal of Cd2 ions from aqueous solutions: adsorption mechanism, kinetics and thermodynamics. Heliyon 5, e02941.

El-Hag Ali, A., Shawky, H.A., El-Sayed, M.H., Ibrahim, H., 2008. Radiation synthesis of functionalized polypropylene fibers and their application in the treatment of some water resources in western desert of Egypt. Sep. Purif. Technol. 63 (2008), 69–76.

Fang, D., Liu, Y., Jiang, S., Nie, J., Ma, G., 2011. Effect of intermolecular interaction on electrospinning of sodium alginate. Carbohydr. Polym. 85 (1), 276–279.

Fanta, F.T., Dubale, A.A., Bebizuh, D.F., Atlabachew, M., 2019. Copper doped zeolite composite for antimicrobial activity and heavy metal removal from waste water. BMC Chemistry 13, 44. https://doi.org/10.1186/s13065-019-0563-1.

Farah, J.Y., El-Gendy, N.S., 2013. Performance, kinetics and equilibrium in biosorption of anionic dye acid red 14 by the waste biomass of Saccharomyces cerevisiae as a low-cost biosorbent. Turkish J Eng Env Sci 37, 146–161.

Farooq, U., Kozinski, J., Ain Khan, M., Athar, M., 2010. Biosorption of heavy metal ions using wheat based biosorbents–a review of the recent literature. Bioresour. Technol. 101, 5043–5053.

Fishman, M.J., Friedman, L.C., 1985. Methods for determination of inorganic substances in water and fluvial sediments, U.S. Geological Survei Book 5, Chapter A1. Open File Report 84:85–495 Denver Colorado U.S.A. for hydrogen isotope analysis. Anal. Chem. 63, 910–912.

Foglar, L., Kljic, M., 2011. The interaction of zeolite and bacterial cells for denitrification of the cetina surface water. Proceedings of the 12th international conference on environmental science and technology Rhodes.

Godfray, H.C., Beddington, J.R., Crute, I.R., Haddad, L., Lawrence, D., Muir, J.F., 2010. Food security: the challenge of feeding 9 billion people. Science 327, 812–818.

Gonzalez, J.S., Martinez, Y.N., Castro, G.R., Alvarez, V.A., 2016. Preparation and characterization of polyvinyl alcohol–pectin cryogels containing enrofloxacin and keratinase as potential transdermal delivery device. Adv. Mater. Lett. 7 (8), 640–645. https://doi.org/10.5185/amlett.2016.6499.

Hem, J.D., 1991. Study and interpretation of the chemical characteristics of natural water. Scientific Publication Jodhpur, India, p. 2254.

Ho, Y.S., McKay, G., 1999. Pseudo-second order model for sorption processes. Process Biochem 34, 451–465.

Hua, S.B., Ma, H.Z., Li, X., Yang, H.X., Wang, A.Q., 2010. pH-sensitive sodium alginate /poly(vinyl alcohol) hydrogel beads prepared by combined Ca2+ crosslinking and freeze-thawing cycles for controlled release of diclofenac sodium. Int. J. Biol. Macromol. 46, 517–523.

Idris, A., Misran, E., Hassan, N., Jalil, A.A., Seng, C.E., 2012. Modified PVA-alginate encapsulated photocatalyst ferro photo gels for Cr(VI) reduction. J. Hazard. Mater. 227–228, 309–316.

Iliescu, R.I., Andronescu, E., Ghitulica, C.D., Voicu, G., Ficai, A., Hoteteu, M., 2014. Montmorillonite-alginate nanocomposite as a drug delivery system—Incorporation and in vitro release of irinotecan. Int. J. Pharm. 463, 184–192.

Isawi, H., 2019. Evaluating the performance of different nano-enhanced ultrafiltration membranes for the removal of organic pollutants from wastewater. J. Water Process Engineering 31 (2019), 100833.

Jahangirian, H., Ismail, M.H.S., Haron, M.J., Soltaninejad, S., 2013. Synthesis and characterization of zeolite/Fe3O4 nanocomposite by green quick precipitation method". Digest J. Nanomater. Biostruct. 8 (4), 1405–1413.

Ji, F., Li, C., Xu, J., Liu, P., 2013. Dynamic adsorption of Cu(II) from aqueous solution by zeolite/cellulose acetate blend fiber in fixed-bed. Colloids Surf. A Physicochem. Eng. Asp. 434, 88–94.

Kobayashi, T., Yoshimoto, M., Nakao, K., 2010. Preparation and Characterization of Immobilized Chelate Extractant in PVA Gel Beads for an Efficient Recovery of Copper (II) in Aqueous Solution. Ind. Eng. Chem. Res. 49, 11652–11660.

Kornicker, W.A., Morse, J.W., 1991. Interactions of divalent cations with the surface of pyrite. Geochim. Cosmochem. Acta 55, 2159–2171.

Kumar, L., Brice, J., Toberer, L., Klein-Seetharaman, J., Knauss, D., Sarkar, S.K., 2019. Antimicrobial biopolymer formation from sodium alginate and algae extract using aminoglycosides. PLoS ONE 14 (3), e0214411. https://doi.org/10.1371/journal.pone.0214411.

Kumar, K.V., Sivanesan, S., Ramamurthi, V., 2005. Adsorption of malachite green onto Pithophora sp., a fresh water algae: equilibrium and kinetic modeling. Process Biochem. 40, 2865–2872.

Lagergren, S., 1898. About the theory of so-called adsorption of soluble substances. Zurtheorie der sogenannten adsorption gelsterstofe, Kungliga Svenska Vetenskapsakademiens, Handlingar 24, 1–39.

Li, Y., Xia, B., Zhao, Q., Liu, F., Du, Q., Wang, D., Li, D., Wang, Z., Zhang, P., Xia, Y., 2011. Removal of copper ions from aqueous solution by calcium alginate immobilized kaolin. J. Environ. Sci. 23, 607–615.

Mahamadi, C., Zambara, P., 2012. Adsorption of Cu(II) from aquatic systems using alginate-immobilized water hyacinth beads. Eur. J. Sci. Res. 71, 581–589.

Moshoeshoe, M., Silas, M., Obuseng, N.-T.V., 2017. A Review of the Chemistry, Structure, Properties and Applications of Zeolites. American J. Mater. Sci. 7 (5), 196–221. https://doi.org/10.5923/j.materials.20170705.12.

Mousavi, H., Hosseynifar, A., Jahed, V., Dehghani, S., 2010. Removal of lead from aqueous solution using waste tire rubber ash as an adsorbent. Braz. J. Chem. Eng. 27, 79–87.

Nakamoto, K., 2006. Infrared and Raman Spectra of Inorganic and Coordination Compounds. Wiley Interscience, New York.

Norton, K., Baskaran, T., 2004. McKenzie, biosorption of zinc from aqueous solutions using biosolids. Adv. Environ. Res. 8, 629–635.

Olmez, H., Arslan, F., Icbudak, H., 2004. Spectrothermal studies on Co(II), Ni(II), Cu(II) and Zn(II) salicylato (1,10-phenanthroline) complexes. J Therm Anal Calorim 76, 793–800.

Park, H.G., Chae, M.Y., 2004. Novel Type of Alginate Gel-based Adsorbents for Heavy Metal Removal. J. Chem. Technol. Biotechnol. 79, 1080–1083.

Payra, P., Dutta, P.K., 2003. Handbook of Zeolite Science and Technology. Marcel Dekker Inc, New York, NY, USA.

Peretz, S., Anghel, D.F., Vasilescu, E., Florea-Spiroiu, M., Stoian, C., Zgherea, G., 2015. Synthesis, Characterization and Adsorption Properties of Alginate Porous Beads. Polym. Bull. 72, 3169–3182.

Petrovic, M., Šoštarić, T., Stojanovi, M., Milojkovic, J., Mihajlovic, M.L., Stanojević, M., Stankovic, S.M., 2016. Removal of Pb^{2+} ions by raw corn silk (Zea mays L.) as a novel biosorbent. J. Taiwan Inst. Chem. Eng. 58, 407–416.

Preetha, B., Viruthagiri, T., 2007. Batch and continuous bisorption of chromium (VI) by Rhizopuc arrhizus. Sep. Purif. Technol. 57, 126–133.

Priya, P.G., Basha, C.A., Ramamurthi, V., Begum, S.N., 2009. Recovery and reuse of Ni(II) from rinse water of electroplating industries. J. Hazard. Mater. 163 (2–3), 899–909.

Quinones, I., Guiochon, G., 1996. Derivation and application of a Jovanovic-Freundlich isotherm model for single-component adsorption on heterogeneous surfaces. J Colloid Interf. Sci. 183, 57–67.

Rafatullah, M., Sulaiman, O., Hashima, R., Ahmad, A., 2009. Adsorption of copper (II), chromium (III), nickel (II) and lead (II) ions from aqueous solutions by meranti sawdust. J. Hazard. Mater. 170, 969–977.

Rafiq, M., Hussain, T., Abid, S., Nazir, A., Masood, R., 2018. Development of sodium alginate/PVA antibacterial nanofibers by

the incorporation of essential oils. Mater. Res. Express 5, (3). https://doi.org/10.1088/2053-1591/aab0b4. doi: 10.1088/2053-1591/aab0b4 035007.

Rahman, N.A., Wilfred, C.D., 2018. Removal of Mn(VII) from Industrial Wastewater by using Alginate-Poly(vinyl) alcohol as Absorbent. J. Phys.: Conf. Ser. 1123, 012067.

F.H. Rainwater, L.L. Thatcher, (1960), Methods for collection and analysis of water samples. U.S. Geological survey water supply, paper 1454. Washington: USGS.

Rezaee, A.A.K.J., Jafari, A.R., Khataee, A., 2011. Niliahmadabadi Escherichia coli removal from water using electro photocatalytic method. J. Appl. Sci. Environ.Manag. 15 (3), 439.

Rihayat, T., Saari, M., Hilmi Mahmood, M., Wan Yunus, W.M.Z., Suraya, A.R., Dahlan, K.Z.H.M., Sapuan, S.M., 2007. Mechanical Characterisation of Polyurethane/Clay Nanocomposites. Polym. Polym. Compos. 15 (8), 647–652.

Rushdi, I., Yousef, M.F., Tutunji, G.A.W., Deraish, S.M.M., 1999. Chemical and structural properties of Jordanian zeolitic tuffs and their admixtures with urea and thiourea: Potential scavengers for phenolics in aqueous medium. J. Colloid Interf. Sci. 216, 348–359. https://doi.org/10.1006/jcis.1999.6334.

Safinejad, A., Goudarzi, N., Arab Chamjangali, M., Bagherian, G., 2017. Effective simultaneous removal of Pb(II) and Cd(II) ions by a new magnetic zeolite prepared from stem sweep. Mater. Res. https://doi.org/10.1088/2053-1591/aa9738.

Sandra, S.K., Blaga, C.R., Aleksandra, K., 2007. Thermal behaviour of Co(II), Ni(II), Cu(II), Zn(II), Hg(II) and Pd(II) complexes with isatin-β-thiosemicarbazone. J. Therm. Anal. Cal. 90, 525–531.

Say, R., Garipcan, B., Emir, S., Patir, S., Denizli, A., 2002. Preparation and characterization of the newly synthesized metal-complexing-ligand N-methacryloylhistidine having PHEMA beads for heavy metal removal from aquouse solutions. Macromol. Mater. Eng. 287, 539–545.

Shalaby, T.H., Eissa, M., El Kady, M., Abd El–Gaber, S., 2018. Geochemistry of El–Salam Canal and the adjacent groundwater in north Sinai, Egypt: an application to a water treatment process using magnetic zeolite nanoparticles. Appl. Water Sci. 8, 105. https://doi.org/10.1007/s13201-018-0741-7.

P. Tirkey, T. Bhattacharya, S. Chakraborty, S. Baraik, 2017. Assessment of groundwater quality and associated health risks: A CASE STUDY OF Ranchi city. India Groundwater for Sustainable Development, Jharkhand.

Wang, K.Y., Chung, T.S., 2006. Fabrication of polybenzimidazole (PBI) nanofiltration hollow fiber membranes for removal of chromate. J. Membr. Sci. 281, 307–315.

Wang, F., Lu, X., Li, X., 2016. Selective removals of heavy metals (Pb^{2+}, Cu^{2+}, and Cd^{2+}) from wastewater by gelation with alginate for effective metal recovery. J. Hazard. Mater. 308, 75–83.

A. Waseem, J. Arshad, F. Iqbal, A. Sajjad, Z. Mehmood, G. Murtaza, 2014. Pollution status of pakistan: a retrospective review on heavy metal contamination of water, soil, and vegetables. Bio Med Research International, vol 2014. Hindawi Publishing Corporation, Cairo, p 29.

Yamaura, K., Kuranuki, N., Suzuki, M., Tanigami, T., Matsuzawa, S., 1990. Properties of mixtures of silk fibroin/syndiotactic-rich poly(vinyl alcohol). J. Appl. Polym. Sci. 41, 2409.

Yang, X., Zhou, T., Ren, B., Hursthouse, A., Zhang, Y., 2018. Removal of Mn (II) by Sodium Alginate/Graphene Oxide Composite Double-Network Hydrogel Beads from Aqueous Solutions. Sci. Rep. 8, 10717. https://doi.org/10.1038/s41598-018-29133-y.

Yin, C.Y., Aroua, M.K., Daud, W.M.A.W., 2007. Review of modification of activated carbon for enhancing contaminant uptakes from aqueous solutions. Sep. Purif. Technol. 52, 403–415.

Yurekli, Y., 2016. Removal of Heavy Metals in Wastewater by Using Zeolite Nano-Particles Impregnated Polysulfone Membranes. J. Hazardous Mater. https://doi.org/10.1016/j.jhazmat.2016.01.064.

Zamzow, M.J., Eichbaum, B.R., Sandgren, K.R., Shanks, D.E., 1990. Removal of Heavy Metals and Other Cations from Wastewater Using Zeolites. Sep. Sci. Technol. 25 (13–15), 1555–1569.

Zendehde, M., Shoshtari-Yeganeh, B., Cruciani, G., 2016. Removal of heavy metals and bacteria from aqueous solution by novel hydroxyapatite/zeolite nanocomposite, preparation, and characterization. J. Iran. Chem. Soc. 13, 1915–1930. https://doi.org/10.1007/s13738-016-0908-9.

Zhan, W., Xu, C., Qian, G., Huang, G., Tang, X., Lin, B., 2018. Adsorption of Cu(II), Zn(II), and Pb(II) from aqueous single and binary metal solutions by regenerated cellulose and sodium alginate chemically modified with polyethyleneimine. RSC Adv. 8, 18723.